iScience

CellPress

Article

Cdc42 Regulates Neuronal Polarity during Cerebellar Axon Formation and Glial-Guided Migration

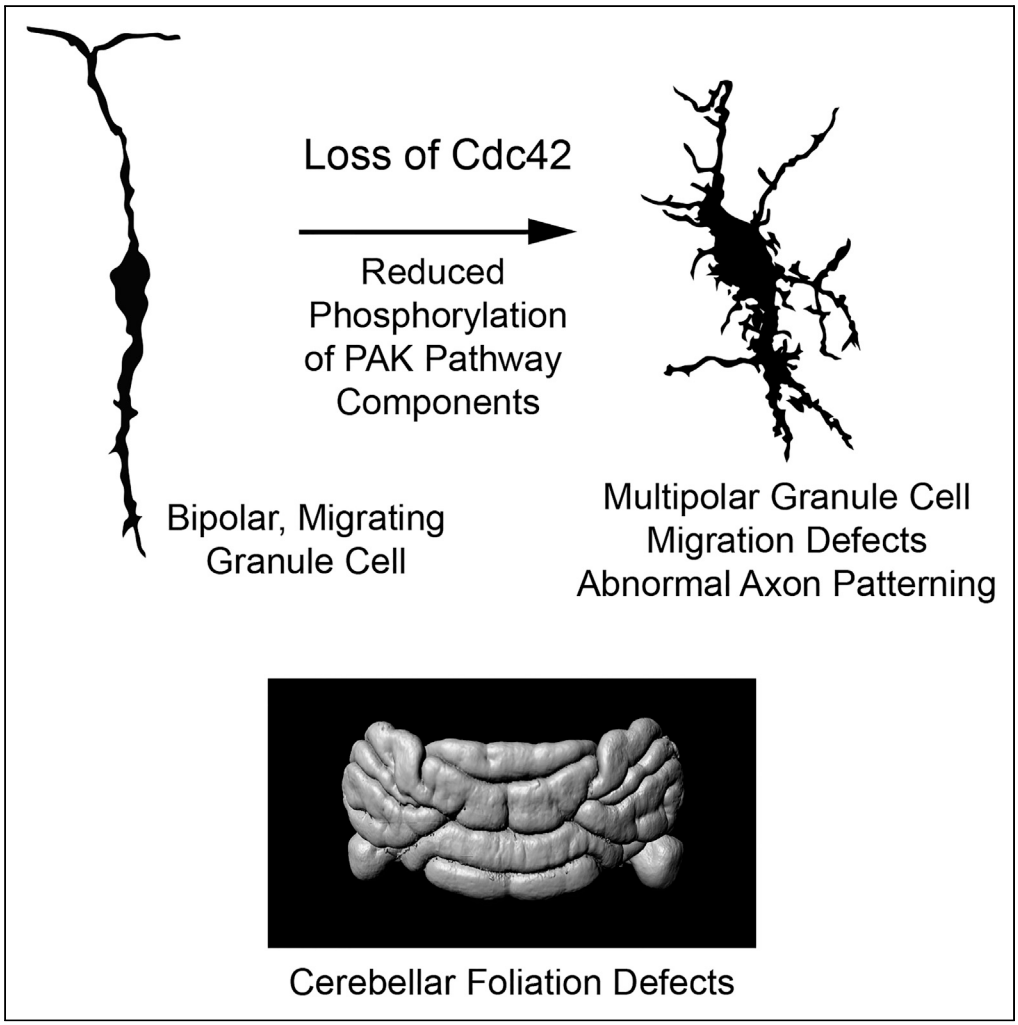

Eve-Ellen Govek, Zhuhao Wu, Devrim Acehan, ..., Yin Fang, Marc Tessier-Lavigne, Mary Elizabeth Hatten

hatten@rockefeller.edu

HIGHLIGHTS

Conditional deletion of *Cdc42* in GCPs perturbs cerebellar cortical histogenesis

Loss of *Cdc42* in GCPs disrupts GCP neuron-glial junctions

Cdc42 deficiency causes a loss of GCP polarity and slows their migration

Phosphoproteomics reveals changes in cytoskeletal, adhesion, and polarity proteins

Govek et al., iScience *1*, 35–48
March 23, 2018
https://doi.org/10.1016/j.isci.2018.01.004

iScience

CellPress

Article

Cdc42 Regulates Neuronal Polarity during Cerebellar Axon Formation and Glial-Guided Migration

Eve-Ellen Govek,[1] Zhuhao Wu,[5] Devrim Acehan,[2] Henrik Molina,[3] Keith Rivera,[4] Xiaodong Zhu,[1] Yin Fang,[1] Marc Tessier-Lavigne,[5,6] and Mary Elizabeth Hatten[1,7,*]

SUMMARY

CNS cortical histogenesis depends on polarity signaling pathways that regulate cell adhesion and motility. Here we report that conditional deletion of the Rho GTPase *Cdc42* in cerebellar granule cell precursors (GCPs) results in abnormalities in cerebellar foliation revealed by iDISCO clearing methodology, a loss of columnar organization of proliferating GCPs in the external germinal layer (EGL), disordered parallel fiber organization in the molecular layer (ML), and a failure to extend a leading process and form a neuron-glial junction during migration along Bergmann glia (BG). Notably, GCPs lacking *Cdc42* had a multi-polar morphology and slowed migration rate. In addition, secondary defects occurred in BG development and organization, especially in the lateral cerebellar hemispheres. By phosphoproteomic analysis, affected Cdc42 targets included regulators of the cytoskeleton, cell adhesion and polarity. Thus, Cdc42 signaling pathways are critical regulators of GCP polarity and the formation of neuron-glial junctions during cerebellar development.

INTRODUCTION

The histogenesis of the laminar architecture of cortical regions of the mammalian brain depends on a finely orchestrated series of developmental processes that includes the migration of post-mitotic neuronal precursors from pseudo-stratified germinal zones to specific layers, where they mature and form synaptic connections with afferent axons. Each step in neuronal development and layer formation depends on characteristic, stage-specific, polarized neuronal morphologies, through coordinated reorganization of the actin and microtubule cytoskeletons. The Rho GTPases control key signaling pathways that regulate cell polarization by interacting with a variety of effector proteins that regulate cytoskeletal dynamics. They have been implicated in every stage of neuronal development, including axon guidance, neuronal migration, dendrite and spine formation, and synaptic plasticity (Azzarelli et al., 2014; Govek et al., 2011). Of the small Rho GTPases, Cdc42 has emerged as a critical regulator of cell polarity and directed cell migrations. As first shown in non-neuronal cells, Cdc42 functions as a critical regulator of cell polarity, centrosome orientation, cell-cell junction formation, and actin dynamics in motile cells (Heasman and Ridley, 2008). During CNS development, *Cdc42* deficiency in telencephalic progenitor cells causes defects in forebrain development (Cappello et al., 2006; Chen et al., 2006). Cdc42 also regulates axon formation (Hall and Lalli, 2010) and dendrite (Scott et al., 2003) and dendritic spine morphogenesis (Kreis et al., 2007). Although electroporation of *Cdc42* mutants *in utero* has been shown to retard radial migration in the developing neocortex (Konno et al., 2005), the function of Cdc42 in the regulation of neuronal polarity in glial-guided CNS migration has not been defined.

The cerebellar cortex has long provided a model for critical steps in cortical histogenesis, including neurogenesis, glial-guided migration, and the formation of neuronal layers. During postnatal cerebellar development, precursors of the granule cell, one of two principal cerebellar neurons, proliferate in the superficial zone of the external germinal layer (EGL) before exiting the cell cycle in the deeper zone of the EGL, where they extend bipolar parallel fiber axons that form synapses with Purkinje cells (PCs), the sole output neuron of the cerebellum. Subsequently, granule cell precursors (GCPs) extend a descending, leading process along radially aligned Bergmann glia (BG), which guides their migration through the molecular layer (ML) (Edmondson and Hatten, 1987; Solecki et al., 2004, 2009). The highly stereotyped sequence of changes in GCP polarity during axon extension, glial-guided migration, and dendrite formation provides a classic paradigm for developmental-stage-specific changes in CNS neuronal polarity (see diagram in Figure S1).

[1]Laboratory of Developmental Neurobiology, The Rockefeller University, New York, NY 10065, USA

[2]The Rockefeller University Electron Microscopy Resource Center, The Rockefeller University, New York, NY 10065, USA

[3]The Rockefeller University Proteomics Resource Center, The Rockefeller University, New York, NY 10065, USA

[4]Mass Spectrometry Shared Resource, Cold Spring Harbor Laboratory, Cold Spring Harbor, NY 11724, USA

[5]Laboratory of Brain Development and Repair, The Rockefeller University, New York, NY 10065, USA

[6]Stanford University, Palo Alto, CA 94305-2061, USA

[7]Lead Contact

*Correspondence: hatten@rockefeller.edu

https://doi.org/10.1016/j.isci.2018.01.004

To examine the function of *Cdc42* in axon patterning and glial-guided migration during cerebellar histogenesis, we conditionally deleted *Cdc42* in cerebellar GCPs. Surprisingly, a conditional loss of *Cdc42* in GCPs caused striking changes in GCP polarity and neuron-glial interactions, as well as thinner, more elongated, and undulated cerebellar folia, the severity of which was revealed by iDISCO methodology. These changes involved deficits in polarity, cell interactions, and motility at each stage of development, including failure to align into pseudo-columns among BG fibers in the proliferative zone, defects in parallel fiber axon fasciculation in the ML, and failure to extend a single, descending leading process along or form a migration junction with BG as they traversed the ML. By phosphoproteomic analyses, changes occurred in the phosphorylation of cytoskeletal, adhesion, and polarity proteins in *Cdc42*-deficient GCPs. Thus, Cdc42 signaling pathways are critical regulators of GCP polarity, neuron-glial interactions, and migration during cerebellar histogenesis.

RESULTS

Expression of Dominant Negative Form of Cdc42 Perturbs GCP Polarity

To examine the role of Cdc42 signaling in cerebellar GCP development, we first over-expressed Venus fluorophore-tagged dominant negative (DN) Cdc42 (Venus-Cdc42N17) to block Cdc42 activity and Venus fluorophore-tagged constitutively active (CA) Cdc42 (Venus-Cdc42V12). We electroporated *Venus-Cdc42N17*, *Venus-Cdc42V12*, or *Venus* alone as a control into postnatal day (P) 8 mouse cerebella and generated organotypic slices of cerebellar cortex. Expression of DN Cdc42 resulted in a dramatic change in GCP morphology. DN Cdc42-expressing cells in the ML, where GCPs undergo glial-guided migration, expressed multiple branched processes (Figure 1B) rather than the classic bipolar morphology of migrating GCPs (Figure 1A). In contrast, after CA Cdc42 expression, some GCPs had small changes in the amount of ruffling of the leading process, but overall, they had a classic bipolar shape, typical of migrating neurons (Figure 1C). These experiments suggested that Cdc42 activity was an important determinant of GCP morphology associated with normal migration along BG fibers.

Conditional Loss of Cdc42 Function Causes Defects in Cerebellar Development

To provide a genetic model for the role of Cdc42 in GCP polarity and cerebellar development, we conditionally deleted *Cdc42* in mouse GCPs by crossing a floxed *Cdc42* line with a *Tg(Atoh1-Cre)* Cre-deleter line (Figures S2A–S2F). P7 *Atoh1-Cre*$^{+/-}$; *Cdc42* $^{loxP/loxP}$ mutant mice lacking *Cdc42* in GCPs had a striking cerebellar phenotype compared with control *Cdc42* $^{loxP/loxP}$ mice with normal Cdc42 levels in GCPs. Overall, the cerebellar shape differed significantly in mutant compared with control animals (stereoscopic images in Figures S2G and S2H). To obtain 3D images of mutant cerebella, we used iDISCO clearing (Liebmann et al., 2016; Renier et al., 2014), immunostained the tissue for the GCP axonal marker TAG1 and the PC marker Calbindin (CALB1), and performed light sheet flourescence microscopy (LSFM). Computer rendering of these images for surface structure revealed the striking undulations of the lateral portions of mutant cerebella compared with the smooth lobes of control cerebella (Figures 1D–1G and S3; File S4). In addition, we observed a fusion of lobes VI–VII in the *Cdc42* cKO. Overall, the mutant cerebellum was longer and thinner than the wild-type cerebellum.

The severity of the lateral undulations in mutant cerebella was also evident in serial, sagittal sections immunostained for GCP and PC markers (Figure S2I). Notably, the lobes in lateral sections were greatly disorganized compared with those of the control. In addition, the presence of more lateral sections in the mutant compared with the control confirmed elongation of the lobes. Sagittal sections of the medial portion of the cerebellum, the vermis, from mutant mice also revealed that the cerebellum was 33% smaller in total area and 23.5% smaller in width in the sagittal plane than those of control mice (Figures 1H–1K).

To study developmental processes, we examined cerebella from embryonic age (E) 16.5 through P15. Sagittal cryostat sections from embryonic and postnatal mice were immunostained with the neuronal marker NeuN and the PC marker CALB1. Although there was no difference in size at E16.5, at later stages, the size of mutant cerebella decreased: 16%, 26%, and 55% at P0, P7, and P15, respectively, compared with control cerebella (Figures S2J–S2Q). As with P7 mice, lateral sagittal sections of P15 mice also revealed an undulating pattern of the principal layers in the lateral aspects of lobes in mutant mice (Figure S2R).

To determine whether changes in cerebellar patterning related to the rate of proliferation of GCPs, we assayed EdU incorporation. Proliferation assays at P7 did not reveal significant changes in the proliferation rate of early postnatal GCPs lacking *Cdc42* (Figures S4A–S4C). Ki67 immunostaining also failed to show

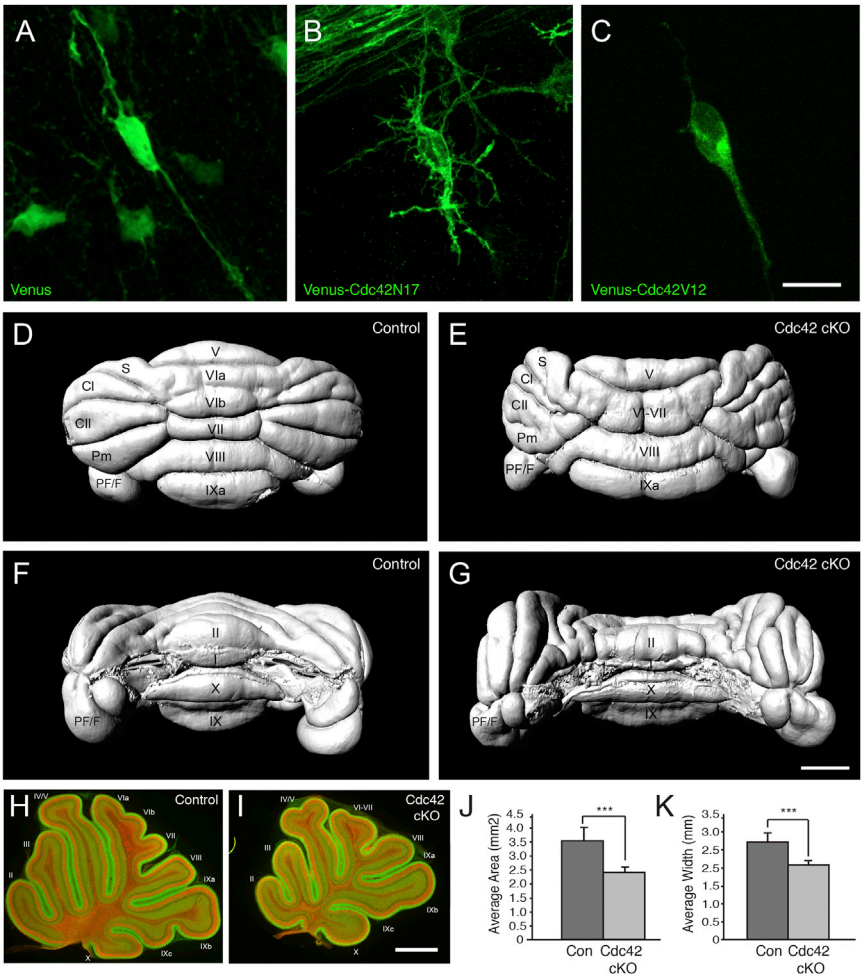

Figure 1. Polarity and Neuroanatomical Changes Caused by Inhibition and Loss of *Cdc42*

(A–C) Inhibition of Cdc42 activity, by electroporating DN Cdc42 (Venus-Cdc42N17, B) into GCPs of P8 wild-type cerebellum and culturing organotypic slices, caused extreme, multiple branching and loss of polarity of GCPs migrating through the molecular layer (ML). Venus control (A) and CA Cdc42 (Venus-Cdc42V12, C) electroporated GCPs exhibited the typical bipolar phenotype of migrating GCPs. Scale bar represents 10 μm.

(D–G) iDISCO clearing, volumetric imaging, and computer rendering of TAG1-immunostained P7 cerebella revealed defects in foliation patterning in the *Cdc42* cKO mutant mouse (E and G) compared with control (D and F). Dorsal images of the cerebellum (D and E). Ventral images of the cerebellum (F and G). Lobes in the vermis are numbered. Lateral hemisphere lobes are labeled S, simplex; CI and II, Crus I and II; Pm, paramedian; PF, paraflocculus; F, flocculus. Scale bar represents 1 mm.

(H–K) Loss of *Cdc42* caused a decrease in the area and width of the cerebellar vermis in the sagittal plane of mutant cerebella (I–K) compared with control cerebella (H, J, and K). Immunostaining for NeuroD1 (green) and β-tubulin (red) was performed to highlight the morphology of the cerebellum. Scale bar represents 500 μm. Data are represented as mean ± SD (***$p < 0.001$).

See also Figures S1–S3 and File S4.

differences in the localization of proliferating GCPs in the outer aspect of the EGL (Figures 2G, 2H, and 4A–4D).

To assess whether the aberrant shape of the cerebellum related to changes in the pattern or rate of cell death during development, we assayed cell death by activated Caspase 3 immunostaining. Again, no significant changes were observed (Figures S4D–S4H). Thus, an autonomous loss of *Cdc42* in GCPs did not affect proliferation during the peak of postnatal GCP proliferation or cell death in the developing cerebellum.

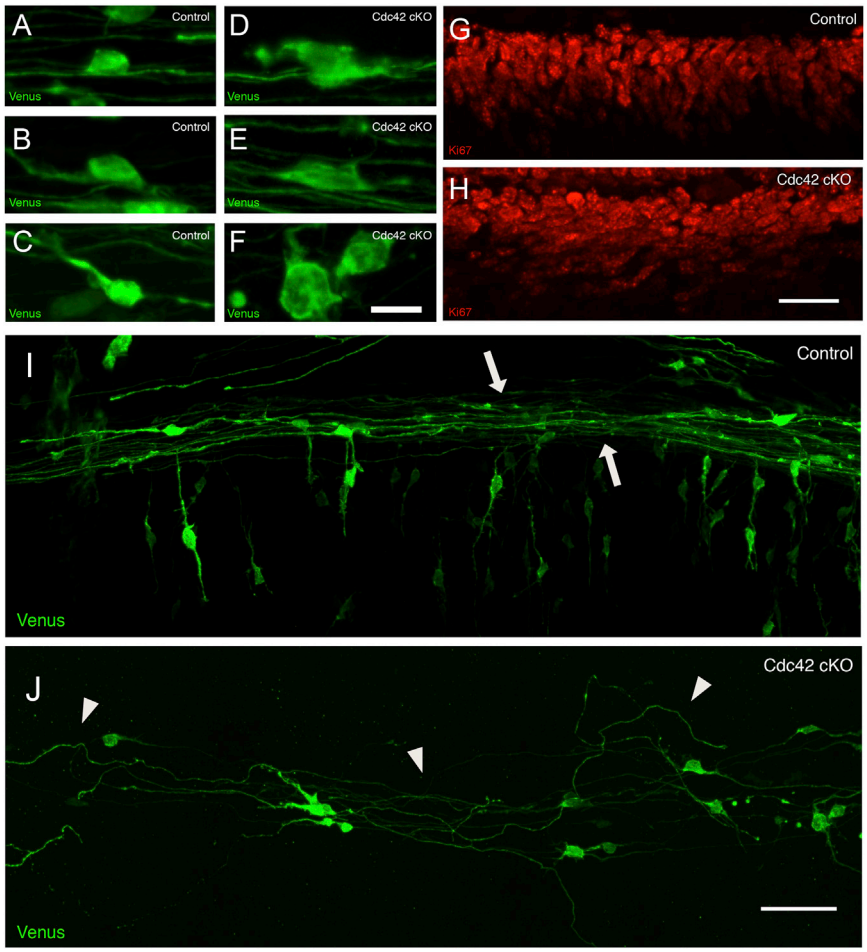

Figure 2. Loss of *Cdc42* Causes Polarity Defects in GCPs in the External Granule Layer of the Cerebellum

(A–F) Venus-expressing GCPs in the EGL of organotypic cerebellar slices of P8 *Cdc42* cKO animals have larger, misshapen cell somas (D–F) compared with those of control animals (A–C). Scale bar represents 10 μm.

(G and H) Immunostaining of P8 mouse sections for Ki67 to label cells in the cell cycle revealed disorganization of the pseudo-columnar arrangement of GCPs in the outer EGL of the cerebellar cortex of *Cdc42* cKO animals (H) compared with control animals (G). Scale bar represents 12.5 μm.

(I and J) Parallel fibers of *Cdc42* cKO GCPs expressing Venus fluorophore (J) are disorganized and defasciculated compared with those of control GCPs (I). Arrows in the control panel indicate the relatively straight and parallel packing of the parallel fibers of control GCPs. Arrowheads in the mutant panel indicate disorganization and lack of fasciculation of the parallel fibers of mutant GCPs. Scale bar represents 50 μm.

See also Figure S1.

Visualization of GCP Developmental Defects by Imaging Venus-Labeled Neurons

To visualize the morphology and cell interactions of developing GCPs in more detail, we used electroporation to express the fluorophore Venus in GCPs in P8 organotypic slices of cerebellar cortex and imaged labeled cells by spinning disc confocal microscopy. After expression of Venus in organotypic slice cultures for 60 hr, a time that would label both proliferating and migrating GCPs, dramatic changes were observed in the polarity of *Cdc42*-deficient GCPs at each developmental stage. Proliferating *Cdc42*-deficient GCPs in the outer aspect of the EGL had irregular, enlarged morphologies (Figures 2D–2F) compared with the classic rounded and/or elongated shapes seen in controls (Figures 2A–2C). Ki67 staining of tissue sections of P8 cerebellum also showed that the nuclei of GCPs lacking *Cdc42* were more rounded (Figures 2G and 2H). Importantly, the organization of proliferating *Cdc42*-deficient GCPs differed dramatically from the controls, where progenitors were arranged in pseudo-columns (Figure 2G). In the *Cdc42* mutant cerebellum, this pseudo-columnar organization was not apparent. Instead, proliferating GCPs were scattered randomly (Figure 2H).

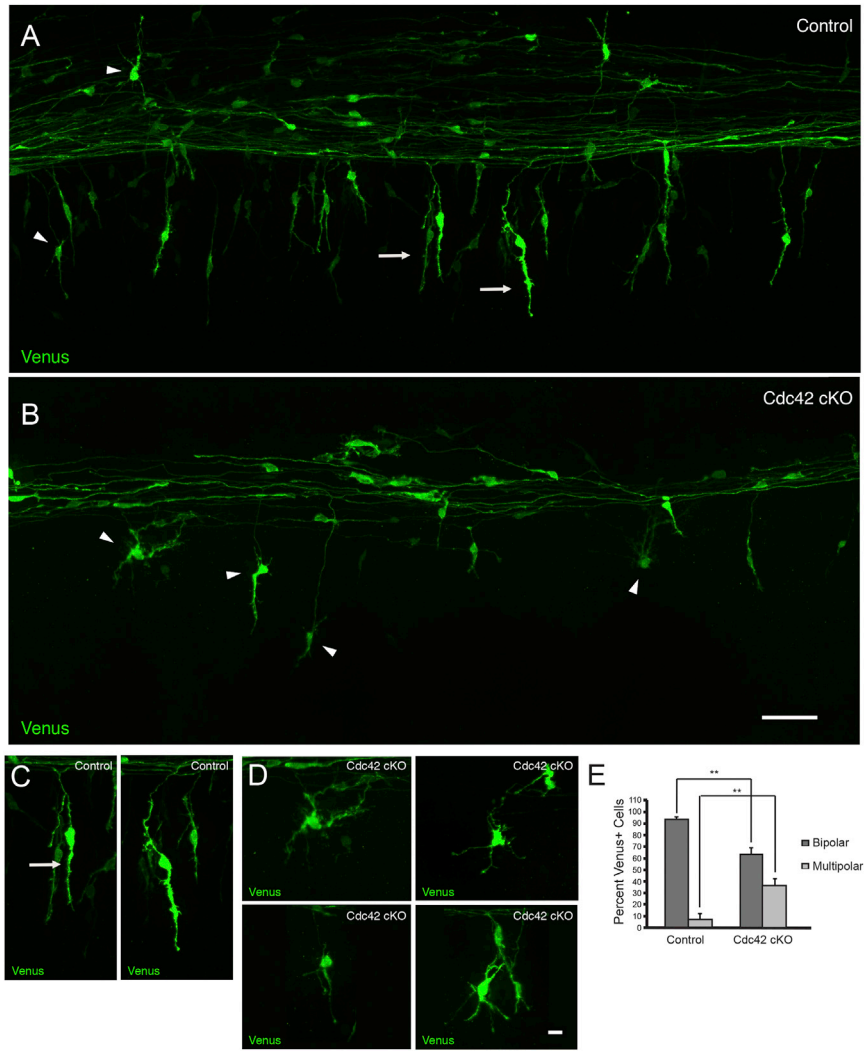

Figure 3. Loss of *Cdc42* Causes Defects in the Polarity of the Leading Process of Migrating GCPs in the Molecular Layer (ML)

(A and B) Venus-expressing control GCPs (A) and *Cdc42* cKO GCPs (B) in organotypic slices of P8 cerebellar cortex. Arrows denote GCPs with a bipolar phenotype. Arrowheads denote GCPs with a multipolar phenotype. Scale bar represents 50 μm.

(C and D) Mutant GCPs tend to be multipolar (D) instead of possessing a single leading process extended in the direction of migration like control GCPs (C). Scale bar represents 10 μm. Arrow denotes GCP with a bipolar phenotype.

(E) Quantitation of the percentage of bipolar and multipolar GCPs in the ML for control and Cdc42 cKO cerebella. Data are represented as mean ± SEM (**$p < 0.01$).

See also Figure S1.

By Venus labeling, although postmitotic *Cdc42*-deficient GCPs extended parallel fiber axons in the deeper aspects of the EGL, they were not fasciculated. Instead GCP parallel fibers coursed in and out of the parallel plane in a highly disorganized manner compared with control GCPs (Figures 2I and 2J). Thus, by confocal imaging, loss of *Cdc42* perturbed GCP axon patterning at early stages of development.

To assay the polarity of migrating GCPs, we imaged labeled cells crossing the ML. The majority of GCPs in the ML of control animals had a bipolar shape with a single leading process in the direction of migration (Figures 3A, 3C, and 3E), whereas many of the Venus-labeled GCPs in the ML of mutant animals were multipolar (Figures 3B, 3D, and 3E). Thus, the morphology of *Cdc42*-deficient GCPs closely resembled that of GCPs that expressed DN Cdc42 (Figures 3B, 3D, and 1B). The loss of classic GCP polarity, especially the

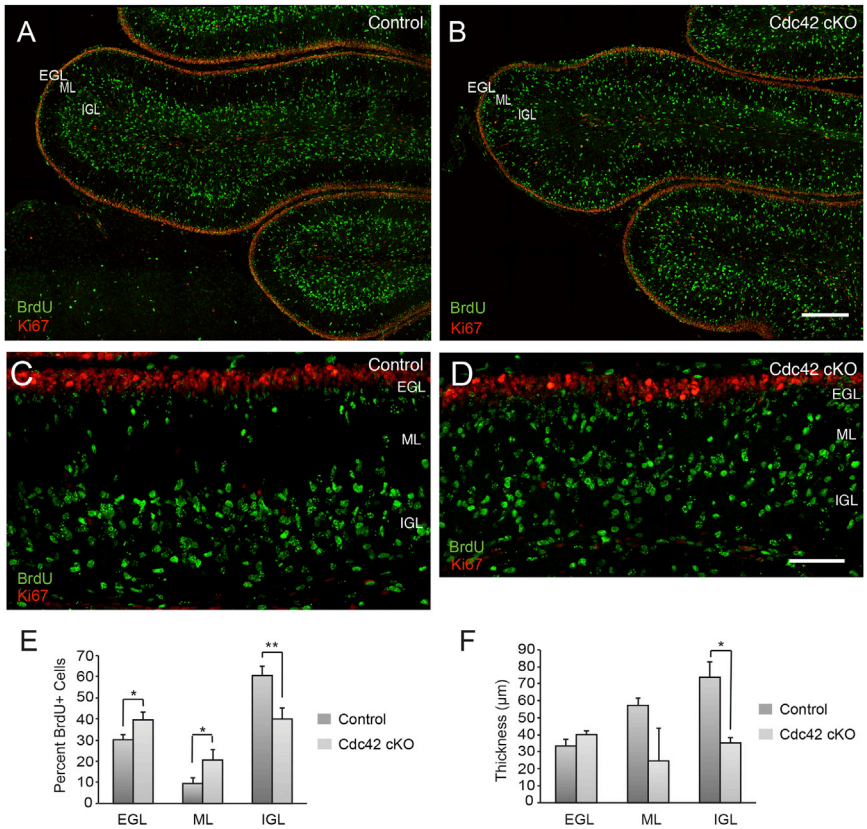

Figure 4. Loss of *Cdc42* Causes Slowed Glial-Guided Migration *In Vivo*

(A–D) Cerebella of P5 control (A and C) and *Cdc42* cKO (B and D) mice were injected with BrdU, and the mice were sacrificed 72 hr later. Immunostaining cerebellar sections for BrdU showed an increased percentage of GCPs in the EGL and ML layers of *Cdc42* cKO animals (B and D) compared with control animals (A and C) and a decreased percentage in the IGL. Immunostaining for Ki67 labeled cells in the cell cycle at the time that the animals were sacrificed. Scale bar for A and B represents 200 µm. Scale bar for C and D represents 50 µm.

(E) Quantitation of BrdU+ cells in the EGL, ML, and IGL of the cerebellar cortex of control and *Cdc42* cKO animals.

(F) Quantitation of the thickness of the different regions of the cerebellar cortex in control and *Cdc42* cKO animals.

Data are represented as mean ± SEM (*$p < 0.05$, **$p < 0.01$).

See also Figure S1.

failure to extend a single, leading process along BG fibers, which is characteristic of migrating GCPs (Edmondson and Hatten, 1987; Gregory et al., 1988), suggested defects in glial-guided migration.

In Vivo Migration Assay of GCPs Lacking Cdc42

To determine the rate of migration of *Cdc42*-deficient GCPs along BG, we used a BrdU incorporation assay. In these experiments, we injected the cerebella of P5 mutant and control mice with BrdU and assayed the distance migrated after 72 hr. Measurements of the distribution of BrdU+ GCPs in the EGL, where proliferation occurs, the ML, where glial-guided migration occurs, and the internal granular layer (IGL), where post-migratory GCPs are located, showed a pronounced decrease in the percentage of post-migratory cells in the IGL (Figures 4A–4E). Thus, BrdU labeling experiments revealed a major delay in GCP migration from the EGL to the IGL.

Secondary Defects in Bergmann Glial Development

Since prior studies showed that defects in GCP axon extension and migration have secondary effects on the development and alignment of BG fibers (Hatten et al., 1984) and GC target neurons, the PCs (Adams et al., 2002), we examined the development of these cells in mutant mice. Loss of *Cdc42* in GCPs had a profound effect on BG fiber morphology in postnatal cerebellum. Control BG aligned their cell bodies in a layer just

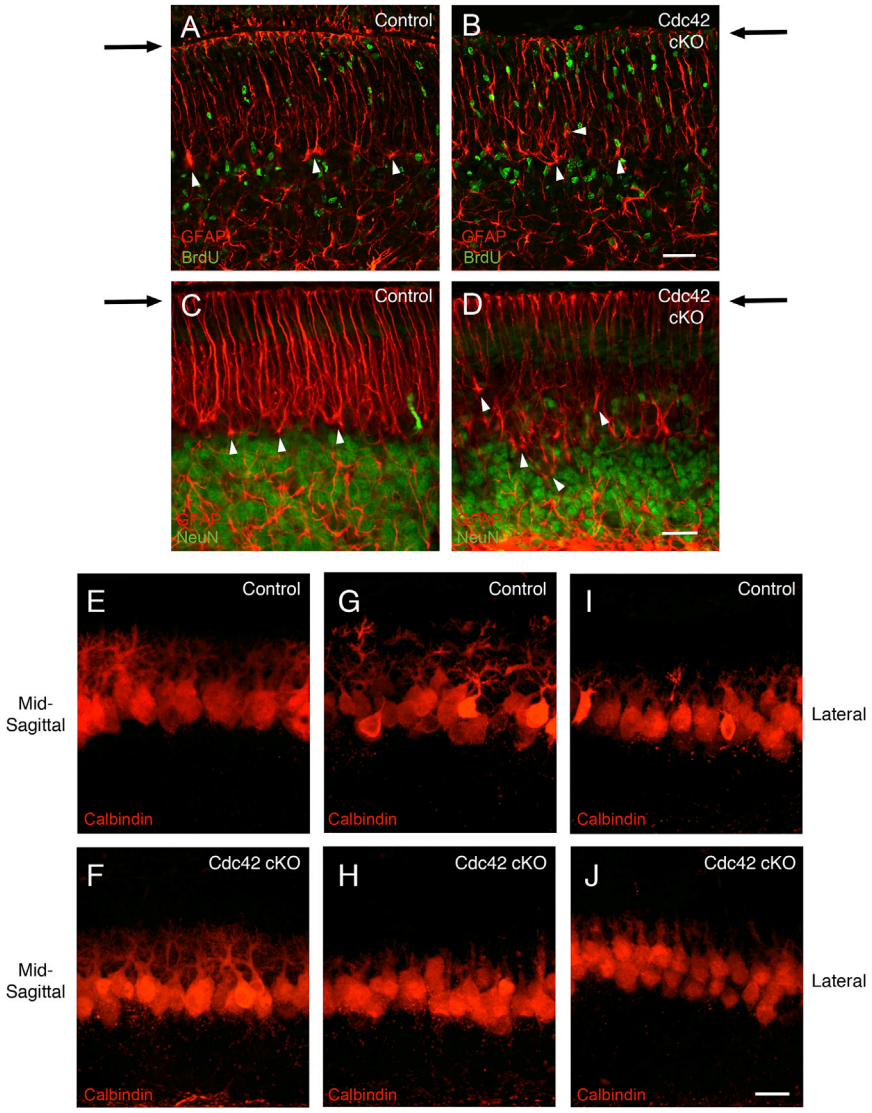

Figure 5. Development of Bergmann Glia and Purkinje Cells in *Cdc42* cKO Mice

(A–D) P8 mid-sagittal (A and B) and lateral (C and D) cerebellar sections from control (A and C) and *Cdc42* cKO (B and D) mice immunostained for GFAP (red) to label glial cells and BrdU (A and B, green) or NeuN (C and D, green) to label GCPs show that GFAP fibers that span the cerebellar cortex in control mice are disorganized in mutant mice. In addition, BG cell bodies, denoted by arrowheads, are mis-localized in *Cdc42* cKO animals and do not align as in control animals. Arrows point to the ends of the glial fibers, which appeared to be thickened and aberrantly fenestrated in *Cdc42* cKO animals compared with control animals. Scale bar for A and B represents 30 μm. Scale bar for C and D represents 25 μm.

(E–J) P8 cerebellar sections were immunostained for calbindin (red) to label PCs in control (E, G, and I) and mutant (F, H, and J) cerebella. PCs in mid-sagittal cerebellar sections were similar in morphology in control (E) and mutant (F) animals, whereas PC dendrites in lateral sections were less elaborate in mutant (H and J) compared with control (G and I) animals. Scale bar represents 25 μm.

See also Figure S5.

below the PCs and extended a radial array of processes to the pial surface (Figures 5A, 5C, and S5A–S5C), whereas the cell bodies of BG in mutant cerebella were mis-localized above and below the PC layer, the processes were often out of the radial plane, and glial end feet were thicker and aberrantly fenestrated compared with those in control mice (Figures 5B, 5D, and S5D–S5F). Defects in BG development and organization were especially prominent in the elongated lateral hemispheres (Figure 5D). Defects in PC morphology and/or alignment were also noted in *Cdc42* cKO animals, with PC dendritic arbors appearing

smaller or tilted out of the sagittal plane and their cell bodies more disorganized compared with those of control cells in lateral cerebellar sections (Figures 5E–5J).

Ultrastructural Features of GCPs Lacking Cdc42: Defects in Neuron-Glial Interactions

To analyze ultrastructural features of neuron-glial interactions of developing GCPs lacking *Cdc42*, we carried out electron microscopy (EM) of P7 cerebella. Strikingly, the BG fibers coursed between the colonnades of GCPs in the EGL, with GCPs apparently aligned among the radial glial fibers (Figure 6A), whereas BG fibers were not apparent in the EGL of the *Cdc42* cKO cerebellum and GCPs were not arranged in a pseudo-columnar pattern (Figure 6B). Instead, irregularly shaped and randomly oriented GCPs were scattered across the EGL among fewer BG fibers that were not strictly radial. Thus, our EM analysis revealed a previously unreported pseudo-columnar pattern of organization in the EGL of control cerebella and an overall loss of this columnar organization in mutant cerebella.

EM analysis of GCPs migrating across the ML also revealed defects in neuron-glial interactions of migrating GCPs, with mutant GCPs failing to form the classic migration junction with BG fibers (Gregory et al., 1988). As reported earlier, BG fibers coursed in and out of the radial plane (Figures 6D, 5B, and 5D). Importantly, GCPs lacking *Cdc42* did not have the characteristic, elongated cell soma closely apposed to BG fibers (Gregory et al., 1988; Rakic, 1971). Instead, GCPs lacking *Cdc42* had irregularly shaped cell somas that were not strictly apposed to glial fibers (Figures 6D, 6D′, and 6F) like control cells (Figures 6C, 6C′, and 6E). Thus, loss of *Cdc42* caused changes in the polarity of GCPs and failure to form a migration junction with BG fibers.

Changes in Gene Expression and Protein Phosphorylation in GCPs Lacking Cdc42

To determine whether changes in GCP polarity, axon patterning, and glial-guided migration related to mPar6 signaling, a key effector of Cdc42, which we previously showed is critical to radial neuronal migration (Solecki et al., 2004), we used Western blotting to probe for changes in mPar6 protein levels or the phosphorylation and thus activation of aPKC, the principle downstream effector of mPar6 signaling, and the aPKC target GSK3β (Figure S6). Surprisingly, no changes in mPar6 levels, aPKC phosphorylation, or GSK3β phosphorylation were detected.

We next took a more global approach and assayed whether loss of *Cdc42* caused general changes in gene transcription. RNA-seq analysis of *Cdc42*-deficient GCPs did not reveal changes in RNA levels for genes involved in cell polarity pathways or neuron-glial interactions (File S1).

Since we did not observe general transcription changes or changes in Par6 levels or activity (Figure S6), we used global phosphoproteomics of P7 GCPs purified from mutant and control cerebella to identify affected phospho targets in *Cdc42*-deficient GCPs. Using a 2-fold cut-off, we identified a decrease in the phosphorylation of 1204 sites corresponding to 740 proteins and an increase in the phosphorylation of 170 sites corresponding to 143 proteins (Table 1 and File S2). Among the proteins identified with changes in phosphorylation were Rho GTPase and Cdc42 regulators and effectors, including Trio, Itsn1, Srgap1/3, and the actin regulatory proteins Pak1/2/4, which are main effector proteins of Cdc42 (Figure S7). A large number of cytoskeletal proteins with changes in phosphorylation were also identified, including Pxn, Fmn2, Dbn1, and Map2. Polarity regulators, such as Numbl and Scrib, also exhibited changes in phosphorylation, as well as a large number of cell adhesion proteins, including α-catenin, σ-catenin, ZO-1, and ZO-2. Biological pathway analysis using the Database for Annotation, Visualization and Integrated Discovery (DAVID) revealed enrichment of phosphorylation sites for "regulation of actin cytoskeleton," "focal adhesion," "tight junction," and "adherens junction," among others (File S3), suggesting that structural changes in the cytoskeleton underlie the changes in polarity and that changes in cell-cell adhesion contribute to the defects in GCP organization, axon fasciculation, and migration in developing GCPs lacking *Cdc42*.

DISCUSSION

The present findings demonstrate a novel, critical role for Cdc42 signaling pathways in key steps in cerebellar histogenesis, including axon patterning, glial-guided migration, and foliation of the cerebellar cortex. At each stage of development, loss of *Cdc42* resulted in defects in neuronal polarity and neuron-glial interactions, including loss of GCP organization in the EGL, disorganized parallel fiber patterning, failure of

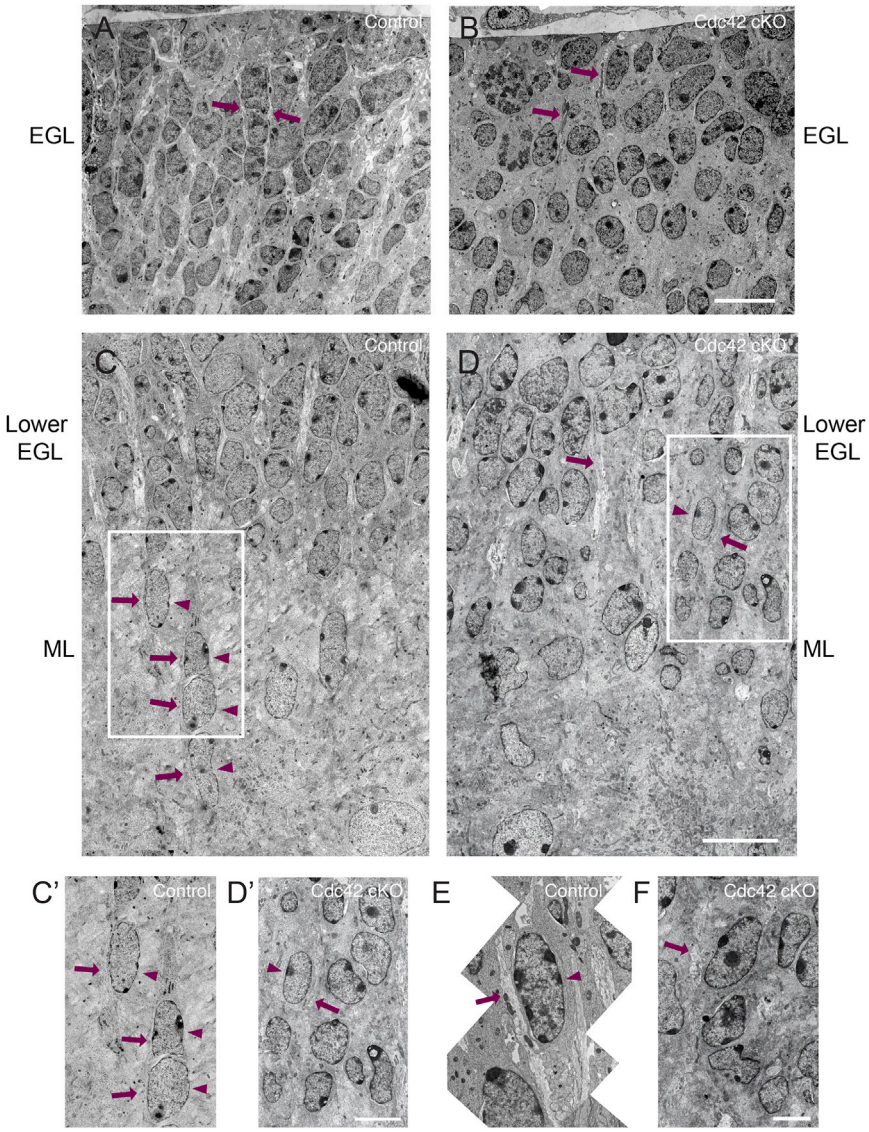

Figure 6. Ultrastructural Features of GCPs Lacking *Cdc42* Revealed Defects in Neuron-Glial Interactions

(A and B) GCPs in control cerebellar cortex (A) were aligned among the radially extended glial fibers, whereas those in mutant cerebellar cortex (B) were scattered randomly throughout the EGL. BG fibers were difficult to detect in the mutant cerebella. Arrows indicate glial fibers. Scale bar represents 10 μm.

(C and D) GCPs lacking *Cdc42* (D) migrating through the molecular layer (ML) had more irregularly shaped nuclei that were not strictly apposed to glial fibers as in the control condition (C). Arrows indicate glial fibers. Arrowhead indicates GCP nucleus apposed to a glial fiber. Scale bar represents 10 μm.

(C′ and D′) Slight zoom of areas boxed in C and D. Note the close apposition of the control cells' nuclei to the glial fiber, whereas the nuclei of most mutant cells near a glial fiber are not aligned with the fiber. Scale bar represents 5 μm. Arrows indicate glial fibers. Arrowheads indicate GCP nuclei apposed to a glial fiber.

(E and F) Zoom of control (E) and mutant (F) GCP migrating through the ML. Note the close apposition of the control cell's nucleus to the glial fiber, whereas the nuclei of mutant cells near a glial fiber are not aligned with the fiber. Scale bar represents 5 μm. Arrows indicate glial fibers. Arrowheads indicate GCP nuclei apposed to a glial fiber.

See also Figure S1.

migrating GCPs to form a leading process along BG fibers, and failure to form a classic migration junction with BG during migration. Unexpectedly, our study also revealed secondary defects in glial fiber organization, which perturbed the apparent organization of proliferating GCPs in the outer EGL and affected

Protein	aa	Position	Down or Up	Localization Prob	Peptide Sequence
Alpha Catenin	S	654	Down	0.97	SRTSVQTEDDQLIAGQSAR
Alpha Catenin	T	657	Down	1.00	SRTSVQTEDDQLIAGQSAR
APC	S	1006	Down	1.00	YSDEQLNSGRQSPSQNER
APC	S	2296	Down	0.98	NSISPGRNGISPPNK
APC	S	2800	Down	0.94	RHSGSYLVTSV
Cortactin	S	370	Down	1.00	KQTPPASPSPQPIEDRPPSSPIYEDAAPFK
Cortactin	S	381	Down	0.80	KQTPPASPSPQPIEDRPPSSPIYEDAAPF
Dcx	S	297	Down	1.00	SPGPMRR
Dcx	S	304	Down	1.00	SKSPADSANGTSSSQLSTPK
Drebrin	T	383	Up	0.84	ALDEVTSSQPPPPPPPPPPTQEAQETTPSLDEELSK
Enah	S	336	Down	0.97	NSRPSSPVNTPSSQPPAAK
Filamin-A	T	1742	Down	0.98	FGGEHVPNSPFQVTALAGDQPTVQTPLR
Formin-2	S	493	Down	0.98	GATADDSGGGSPVLAAK
Ncam1	T	757	Down	0.97	EPIVEVRTEEERTPNHDGGK
Numbl	S	263	Down	1.00	KAEAAAAPAVAPGPAQPGHVSPTPATTSPGEK
Numbl	S	305	Down	1.00	QGSFRGFPALSQK
Pak1	S	222	Down	0.98	SVIEPLPVTPTRDVATSPISPTENNTTPPDALTR
Pak2	S	141	Down	1.00	YLSFTPPEK
Pak2	S	197	Down	1.00	SVIDPIPAPVGDSNVDSGAK
Pak4	S	104	Down	1.00	RESPPPPAR
Pak4	S	181	Down	1.00	RPLSGPDVSTPQPGSLTSGTK
Pak4	S	293	Down	1.00	ALAAPAVPPAPGPPGPRSPQREPQR
Paxillin	S	244	Down	0.89	GLEDVRPSVESLLDELESSVPSPVPAITVNQGEMSSPQR
Srgap1	S	906	Down	1.00	GLNNDSPERR
Wipf2	S	235	Down	1.00	LHPGREGHPAPPPVKPPPSPVNIR

Table 1. Phosphoproteomics of *Cdc42*-Deficient GCPs

Table of phosphorylation sites that changed 2-fold or more for selected Cdc42, cytoskeletal, and adhesion-related proteins. The protein name is provided, and the identity of the phosphorylated amino acid (aa) is given as serine (S) or threonine (T). The position of the phosphorylated aa in the protein sequence is given, as well as whether the phosphorylation is upregulated (Up) or downregulated (Down). The localization probability is the probability that the identified residue is the correct phosphorylation site, and the matched peptide sequence is provided. For proteins of interest, all phosphorylation sites are shown if multiples were detected.See also Figure S7 and Files S2 and S3.

cerebellar folia formation. Molecular analyses of downstream signaling pathways in GCPs lacking *Cdc42* revealed changes in the phosphorylation of prominent Cdc42 signaling proteins, including the actin regulatory proteins Pak1/2/4.

The changes we observed in the cerebellar cortex patterning of *Cdc42* cKO animals, a decrease in width and elongation in length with severe undulation of the lateral lobes, have not been reported previously. These changes were especially apparent in iDISCO clearing and LSFM imaging of whole cerebellum, which revealed the extent of the undulation of the lateral lobes and the fusion of lobes VI–VII. The increase in overall length was also supported by an increased number of serial sections of mutant cerebella compared with controls. Although the thinner folia and smaller area and width of mid-sagittal sections of mutant cerebella

gave the appearance of a smaller cerebellum, the increased length of folia suggested that the overall size of the cerebellum did not change, which is consistent with our finding that proliferation rates at the peak of GCP proliferation did not change. The surface rendering provided by the iDISCO/LSFM methodology used in this study is a critical advance for analyzing foliation patterning during cortical histogenesis. Previously, this level of detail was only possible with MRI imaging.

The changes we observed in foliation patterning likely relate to changes in the timing of neuronal migration and subsequent secondary defects in BG organization, which possibly affected neuron-glial interactions involved in migration and PC development. This interpretation is consistent with the fact that defects in BG fiber orientation in mutant cerebellum were most pronounced in the lateral hemispheres where foliation defects were also observed. Notably, defects in PC dendritic arborization and alignment were also seen in the lateral hemispheres of the cerebellum. The defects in PC dendritic arborization could relate to slowed GC migration (Adams et al., 2002), which would alter the dynamics of parallel fiber-PC synapse formation, or to secondary defects in BG, as PC dendritic orientation is thought to relate, at least in part, to contacts with BG. As discussed later, these secondary defects likely emanate from loss of Cdc42 function in GC polarity and adhesions required to maintain BG development.

The present study revealed a previously unreported organization of proliferating GCPs into pseudo-columns among radially aligned BG fibers in the external EGL. This organization was lost in *Cdc42*-deficient GCPs, apparently because of both a change in GCP polarity from small, rounded cells to irregularly shaped cells, and more importantly because of secondary, non-autonomous effects on BG fiber organization, which skewed the glial fibers out of the radial plane in mutant cerebellum. Defects in both glial cell body localization and radial orientation of BG fibers were apparent in light microscopy and EM of cerebella with *Cdc42*-deficient GCPs. The conclusion that defects in BG development were secondary to loss of neuron-glial interactions is consistent with prior studies showing secondary defects in BG development in the cerebellum of mice with autonomous neuronal defects in neuron-glial interactions, such as the *weaver* mouse (Hatten et al., 1984). As we did not observe changes in the number of EdU or Ki67-labeled cells in *Cdc42*-deficient GCPs, the defects in the columnar arrangement of proliferative GCPs did not correlate with significant changes in the proliferation of GCPs in the EGL, the zone where neurogenesis occurs. This result is in contrast to studies on the role of Cdc42 in cortical neurogenesis, where loss of *Cdc42* resulted in defects in the position of mitoses, cell fate, and localization of cortical progenitors (Cappello et al., 2006; Chen et al., 2006).

Although *Cdc42*-deficient GCPs formed parallel fibers, striking defects in parallel fiber fasciculation, which organizes them into the classic parallel array, occurred in the absence of Cdc42 activity. Some insights into the defects in parallel fiber fasciculation observed can perhaps be gained from the results of our RNA-Seq and phosphoproteomic assays. Known regulators of axon fasciculation include cadherins and Ncam proteins. Interestingly, we observed an increase in mRNA expression of *Fat2*, an atypical cadherin capable of homophilic interactions that localizes to GCP parallel fibers (Nakayama et al., 2002) in our RNA-Seq analysis. We also found a decrease in the phosphorylation of the neural cell adhesion molecule Ncam1, which has been implicated in cell-cell adhesion, neurite outgrowth, synaptic plasticity, and learning and memory and interacts with the neuronal cytoskeleton. It is also possible that loss of Cdc42 activity affected the regulation of actin dynamics that control growth cone motility along parallel fiber tracts. These defects in parallel fiber packing could have affected GCP contacts with PCs, causing the secondary defects in PC development and alignment in the lateral hemispheres of the cerebellum of mutant mice, and they are consistent with prior studies showing secondary defects in PC development and alignment in the cerebellum of *Astn1* null mice (Adams et al., 2002). Our findings on cerebellar GCP axon extension differ from results of studies on hippocampal neurons, where loss of *Cdc42* or perturbation of Cdc42 activity and signaling using CA and DN Cdc42 mutants impaired axon formation (Garvalov et al., 2007; Schwamborn and Puschel, 2004).

The most striking change in GCP polarity and motility was that *Cdc42*-deficient GCPs had multipolar, branched processes rather than the classic bipolar descending process seen in GCPs migrating along BG fibers (Edmondson and Hatten, 1987; Gregory et al., 1988). This prominent change in polarity occurred in spite of the fact that GCPs lacking *Cdc42* formed a T-shaped axon similar to control GCPs in cerebellar slices. The finding that expression of DN Cdc42 *in vivo* resulted in defects in

the polarity of GCPs quite similar to those seen in GCPs with a conditional deletion of *Cdc42* supports our interpretation that Cdc42 activity is required to express the classic morphology of migrating cerebellar granule cells. Although perturbation of Cdc42 activity in cortical precursors impairs radial migration (Konno et al., 2005), the present study is the first indication that Cdc42 activity regulates both the extension of a leading process and the formation of a migration junction with the glial fiber during CNS neuronal migration.

The results of our BrdU assays indicate, that *Cdc42*-deficient GCPs had a slowed rate of migration through the ML. Since prior studies showed that the mPar6 signaling complex regulates coordinated movement of the centrosome and cell soma during migration (Solecki et al., 2004), we anticipated that Cdc42 activity would regulate Par6 and PKCζ activity in GCPs. This was apparently not the case, as loss of Cdc42 activity did not alter Par6 expression or aPKC phosphorylation in GCPs. However, our phosphoproteomic analysis of *Cdc42*-deficient GCPs suggested that cytoskeletal and adhesion pathways were the molecular pathways underlying the changes in GCP organization, polarization, and migration that we observed.

Global phosphoproteomics is a powerful means to reveal signaling pathway networks, as well as identify specific targets and effectors, including those of small Rho GTPases (Gnad et al., 2013; Nishioka et al., 2012). In the present study, pathway analysis of the global phosphorylation changes we observed after deletion of *Cdc42* in GCPs identified principal pathways likely to function in GCP polarity, axon fasciculation, and migration, including "regulation of actin cytoskeleton," "focal adhesion," "tight junction," and "adherens junction" (File S3). We identified changes in a number of Rho GTPase and Cdc42 regulators, including Trio, Itsn1, and Srgap1/3. Of the main effector proteins of Cdc42 (Figure S7), we identified changes in the phosphorylation of Pak1/2/4, as well as a number of cytoskeletal proteins that are Pak targets, including Pxn, Cttn, Flna, and Stmn1. We also identified a number of cell adhesion molecules, including classical adhesion proteins, such as α-catenin, σ-catenin, ZO-1, and ZO-2. Although we identified Numbl and Scrib polarity proteins among those with decreases in phosphorylation, other regulators of polarity, such as the Pak proteins, Trio and Pxn, were also identified. Taken together, the large number of cytoskeletal and adhesion proteins affected in our phosphoproteomic analysis underscores the importance of Cdc42 activity in cytoskeletal dynamics during the polarization and extension of the leading process during glial-guided migration and cell adhesion required for cell organization and migration.

The current study underscores the importance of Cdc42 signaling to neuronal polarity and cell-cell interactions required for parallel fiber axon patterning and glial-guided migration during cerebellar development. The loss of *Cdc42* signaling had a dramatic effect on GCP development with secondary effects on BG development, resulting in unique changes in the overall length and width of the cerebellum. Importantly, our studies revealed a previously unappreciated role for BG fibers in the organization of GCPs into pseudo-columns within the EGL. Although it will be important to further analyze the roles of Cdc42 targets identified in our phosphoproteomic analysis, it is clear that Cdc42 affects many signaling pathways that converge to organize cerebellar histogenesis. Understanding the role of Rho GTPase signaling in cortical development will likely provide important insights on the assembly of CNS circuits and behavior.

METHODS

All methods can be found in the accompanying Transparent Methods supplemental file.

DATA SOFTWARE AND AVAILABILITY

All raw LC-MS/MS data and peptide identifications have been uploaded to the PRIDE data repository: Project Name: Cdc42 phosphorylation study, Project accession: PXD008148, Username: reviewer79582@ebi.ac.uk, Password: WILJxtep All. RAW files and matched peptides were deposited at PRIDE.

SUPPLEMENTAL INFORMATION

Supplemental Information includes Transparent Methods, seven figures, and four data files and can be found with this article online at https://doi.org/10.1016/j.isci.2018.01.004.

ACKNOWLEDGMENTS

We are especially grateful to Dr. Linda Van Aelst at Cold Spring Harbor Laboratory for critical discussions on these experiments and for providing CA and DN *Cdc42* cDNAs, Dr. Carol A. Mason at Columbia for critical comments on the electron microscopy, and Dr. Alexandra Joyner at Memorial Sloan Kettering Cancer Center (MSKCC) for advice on foliation patterning and defects. We thank Dr. Yi Zheng at Cincinnati Children's Hospital for the floxed *Cdc42* mice and Dr. David Rowitch at UCSF and Dr. Alex Joyner at MSKCC for providing the *Atoh1-Cre* mice. Drs. Linda Van Aelst, David J. Solecki, Hourinaz Behesti, and Zachi Horn provided critical comments on the manuscript and reviewed the phosphoproteomic data. We thank Drs. Brian Chait at The Rockefeller University and Darryl Pappin of Cold Spring Harbor Laboratory for advice on our phosphoproteomic analysis. Dr. Kunihiro Uryu of The Rockefeller University Electron Microscopy Resource Center provided help with the electron microscopy. We also thank Dr. Connie Zhao of The Rockefeller Genomics Resource Center for performing the RNA sequencing and Dr. Nicolas Robine of the New York Genome Center (NYGC) and Dr. Yupu Liang of the Rockefeller CCTS Bioinformatics Program for performing bioinformatic analysis of the RNA-seq data. We thank Weslie Janeway for making and preparing DNA constructs and Raquel Hernandez-Solis and Rebecca de Frates for analyzing cerebellar morphology and size at different developmental stages. This work was supported by NIH grant R01 5R01NS051778-09 (M.E.H.) and a grant from the Eugene W. Chinery 2012 Trust (M.E.H.).

AUTHOR CONTRIBUTIONS

M.E.H. and E.-E.G. designed all experiments and wrote the manuscript. E.-E.G. carried out the anatomical analyses, light microscopy, and biochemical assays. M.T.-L. and Z.W. designed and carried out the iDISCO clearing and LSFM. D.A. carried out the electron microscopy, H.M. carried out the global phosphoproteomics, and K.R. did the bioinformatics analysis of the phosphoproteomic datasets. X.Z. assisted with phosphoproteomic and Western blotting analyses, and Y.F. assisted with BrdU assays, immunohistochemistry, and mouse husbandry.

DECLARATION OF INTERESTS

The authors declare no competing interests.

Received: September 6, 2017
Revised: January 2, 2018
Accepted: January 31, 2018
Published: March 8, 2018

REFERENCES

Adams, N.C., Tomoda, T., Cooper, M., Dietz, G., and Hatten, M.E. (2002). Mice that lack astrotactin have slowed neuronal migration. Development *129*, 965–972.

Azzarelli, R., Kerloch, T., and Pacary, E. (2014). Regulation of cerebral cortex development by Rho GTPases: insights from in vivo studies. Front. Cell. Neurosci. *8*, 445.

Cappello, S., Attardo, A., Wu, X., Iwasato, T., Itohara, S., Wilsch-Brauninger, M., Eilken, H.M., Rieger, M.A., Schroeder, T.T., Huttner, W.B., et al. (2006). The Rho-GTPase cdc42 regulates neural progenitor fate at the apical surface. Nat. Neurosci. *9*, 1099–1107.

Chen, L., Liao, G., Yang, L., Campbell, K., Nakafuku, M., Kuan, C.Y., and Zheng, Y. (2006). Cdc42 deficiency causes Sonic hedgehog-independent holoprosencephaly. Proc. Natl. Acad. Sci. USA *103*, 16520–16525.

Edmondson, J.C., and Hatten, M.E. (1987). Glial-guided granule neuron migration in vitro: a high-resolution time-lapse video microscopic study. J. Neurosci. *7*, 1928–1934.

Garvalov, B.K., Flynn, K.C., Neukirchen, D., Meyn, L., Teusch, N., Wu, X., Brakebusch, C., Bamburg, J.R., and Bradke, F. (2007). Cdc42 regulates cofilin during the establishment of neuronal polarity. J. Neurosci. *27*, 13117–13129.

Gnad, F., Young, A., Zhou, W., Lyle, K., Ong, C.C., Stokes, M.P., Silva, J.C., Belvin, M., Friedman, L.S., Koeppen, H., et al. (2013). Systems-wide analysis of K-Ras, Cdc42, and PAK4 signaling by quantitative phosphoproteomics. Mol. Cell. Proteomics *12*, 2070–2080.

Govek, E.E., Hatten, M.E., and Van Aelst, L. (2011). The role of Rho GTPase proteins in CNS neuronal migration. Dev. Neurobiol. *71*, 528–553.

Gregory, W.A., Edmondson, J.C., Hatten, M.E., and Mason, C.A. (1988). Cytology and neuron-glial apposition of migrating cerebellar granule cells in vitro. J. Neurosci. *8*, 1728–1738.

Hall, A., and Lalli, G. (2010). Rho and Ras GTPases in axon growth, guidance, and branching. Cold Spring Harb. Perspect. Biol. *2*, a001818.

Hatten, M.E., Liem, R.K., and Mason, C.A. (1984). Defects in specific associations between astroglia and neurons occur in microcultures of weaver mouse cerebellar cells. J. Neurosci. *4*, 1163–1172.

Heasman, S.J., and Ridley, A.J. (2008). Mammalian Rho GTPases: new insights into their functions from in vivo studies. Nat. Rev. Mol. Cell Biol. *9*, 690–701.

Konno, D., Yoshimura, S., Hori, K., Maruoka, H., and Sobue, K. (2005). Involvement of the phosphatidylinositol 3-kinase/rac1 and cdc42 pathways in radial migration of cortical neurons. J. Biol. Chem. *280*, 5082–5088.

Kreis, P., Thevenot, E., Rousseau, V., Boda, B., Muller, D., and Barnier, J.V. (2007). The p21-activated kinase 3 implicated in mental retardation regulates spine morphogenesis through a Cdc42-dependent pathway. J. Biol. Chem. *282*, 21497–21506.

Liebmann, T., Renier, N., Bettayeb, K., Greengard, P., Tessier-Lavigne, M., and Flajolet, M. (2016). Three-dimensional study of Alzheimer's disease hallmarks using the

iDISCO clearing method. Cell Rep. *16*, 1138–1152.

Nakayama, M., Nakajima, D., Yoshimura, R., Endo, Y., and Ohara, O. (2002). MEGF1/fat2 proteins containing extraordinarily large extracellular domains are localized to thin parallel fibers of cerebellar granule cells. Mol. Cell. Neurosci. *20*, 563–578.

Nishioka, T., Nakayama, M., Amano, M., and Kaibuchi, K. (2012). Proteomic screening for Rho-kinase substrates by combining kinase and phosphatase inhibitors with 14-3-3zeta affinity chromatography. Cell Struct. Funct. *37*, 39–48.

Rakic, P. (1971). Neuron-glia relationship during granule cell migration in developing cerebellar cortex. A Golgi and electron microscopic study in Macacus Rhesus. J. Comp. Neurol. *141*, 283–312.

Renier, N., Wu, Z., Simon, D.J., Yang, J., Ariel, P., and Tessier-Lavigne, M. (2014). iDISCO: a simple, rapid method to immunolabel large tissue samples for volume imaging. Cell *159*, 896–910.

Schwamborn, J.C., and Puschel, A.W. (2004). The sequential activity of the GTPases Rap1B and Cdc42 determines neuronal polarity. Nat. Neurosci. *7*, 923–929.

Scott, E.K., Reuter, J.E., and Luo, L. (2003). Small GTPase Cdc42 is required for multiple aspects of dendritic morphogenesis. J. Neurosci. *23*, 3118–3123.

Solecki, D.J., Model, L., Gaetz, J., Kapoor, T.M., and Hatten, M.E. (2004). Par6alpha signaling controls glial-guided neuronal migration. Nat. Neurosci. *7*, 1195–1203.

Solecki, D.J., Trivedi, N., Govek, E.E., Kerekes, R.A., Gleason, S.S., and Hatten, M.E. (2009). Myosin II motors and F-actin dynamics drive the coordinated movement of the centrosome and soma during CNS glial-guided neuronal migration. Neuron *63*, 63–80.

ISCI, Volume *1*

Supplemental Information

Cdc42 Regulates Neuronal Polarity during Cerebellar Axon Formation and Glial-Guided Migration

Eve-Ellen Govek, Zhuhao Wu, Devrim Acehan, Henrik Molina, Keith Rivera, Xiaodong Zhu, Yin Fang, Marc Tessier-Lavigne, and Mary Elizabeth Hatten

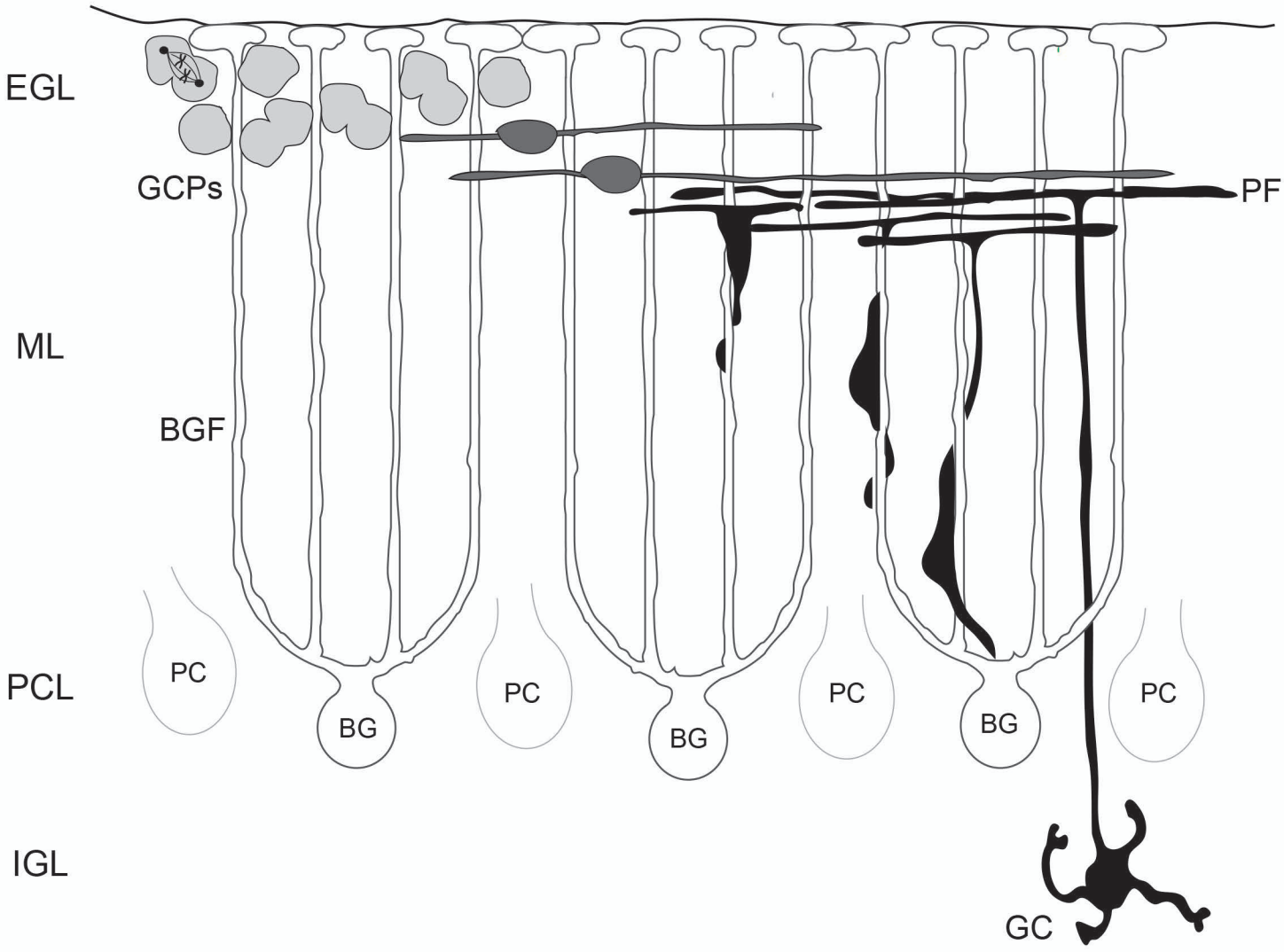
EGL
GCPs
PF
ML
BGF
PCL
PC
BG
PC
BG
PC
BG
PC
IGL
GC

Figure S1. Diagram for Granule Cell Progenitor (GCP) Development in Postnatal Cerebellar Cortex. Related to Figure 1, 2, 3, 4, and 6.

Granule Cell Progenitors (GCPs) proliferate in the superficial zone of the external germinal layer (EGL). They then exit the cell cycle in the deeper zone of the EGL, where they extend bipolar parallel fiber axons (PF), which form synapses with Purkinje cells (PC). Subsequently, GCPs extend a descending, leading process along radially aligned Bergmann glial fibers (BGF) of Bergmann glial cells (BG), and migrate through the molecular layer (ML), past the Purkinje cell layer (PCL), and into the internal granule cell layer (IGL), where mature granule cells (GC) extend short, claw-like dendrites that form synaptic contacts with ingrowing mossy fiber afferents.

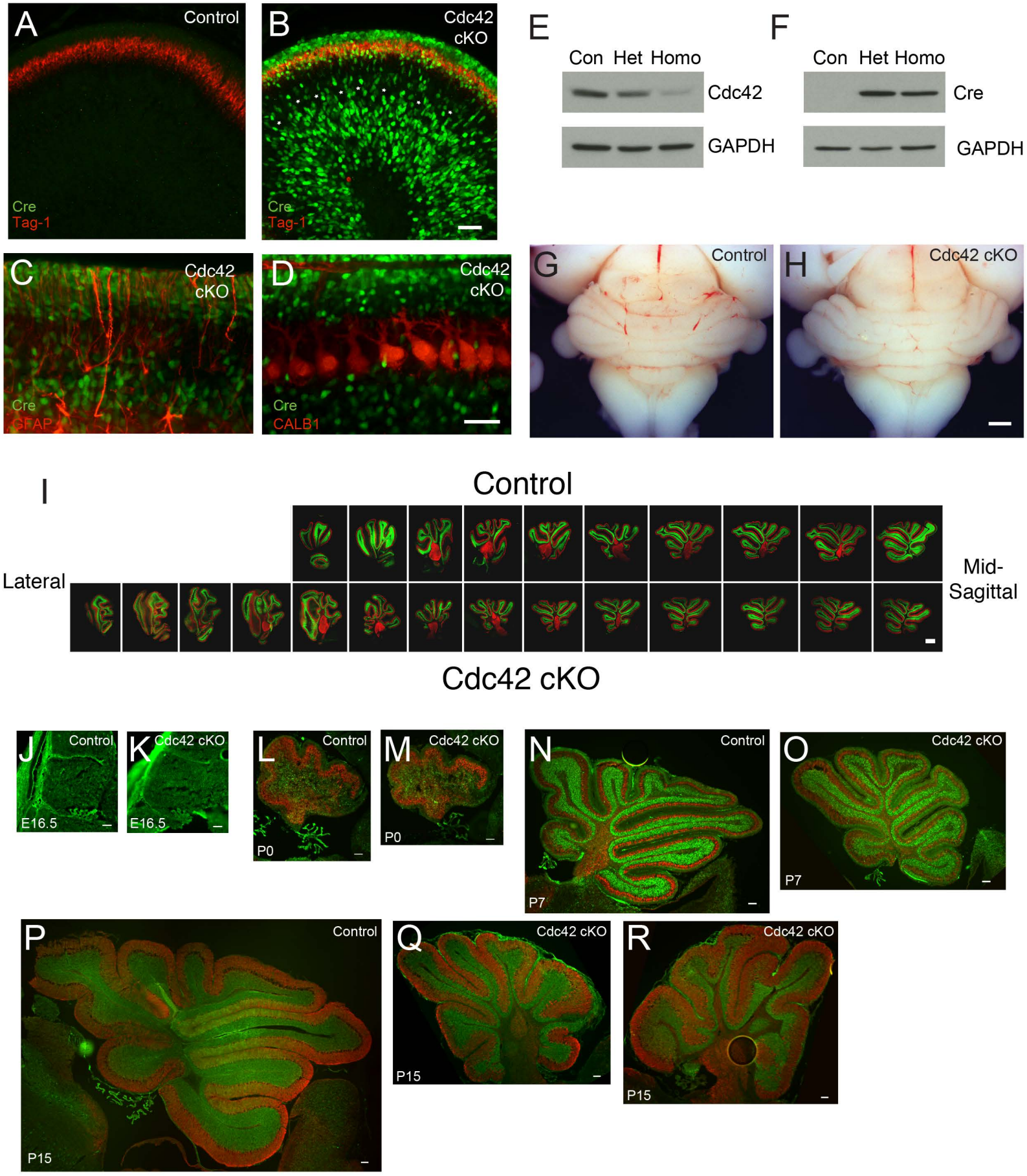
A
Control
Cre
Tag-1
B
Cdc42
cKO
Cre
Tag-1
E
Con Het Homo
Cdc42
GAPDH
F
Con Het Homo
Cre
GAPDH
C
Cdc42
cKO
Cre
GFAP
D
Cdc42
cKO
Cre
CALB1
G
Control
H
Cdc42 cKO
I
Control
Lateral
Mid-
Sagittal
Cdc42 cKO
J
Control
E16.5
K
Cdc42 cKO
E16.5
L
Control
P0
M
Cdc42 cKO
P0
N
Control
P7
O
Cdc42 cKO
P7
P
Control
P15
Q
Cdc42 cKO
P15
R
Cdc42 cKO
P15

Figure S2. Confirmation of Cre expression in GCPs from Cdc42 cKO Cerebella and Changes in Cerebellar Shape and Size over Development. Related to Figure 1.

(A and B) Cre and Tag-1 immunostaining of control (A) and *Cdc42* cKO (B) mid-sagittal cryostat sections. Scale bar for A and B, 25 μm.

(C) Cre and GFAP immunostaining of *Cdc42* cKO mid-sagittal cryostat section shows that Cre is not expressed in glial cells.

(D) Cre and CALB1 immunostaining of *Cdc42* cKO mid-sagittal cryostat section shows that Cre is not expressed in PCs. Scale bar for C and D, 30 μm.

(E and F) Western blots of GCPs isolated from control (Con), *Cdc42* heterozygote (Het) and *Cdc42* homozygote (Homo) mice to show loss of Cdc42 expression (E) when Cre is expressed (F).

(G and H) Stereo microscopic images of control and *Cdc42* cKO cerebella revealed a narrower, longer mutant cerebellum with undulating lateral lobes (H) compared to the full, straight lobes of the control (G). Scale bar, 500 μm.

(I) Serial sagittal sections of control (top) and mutant (bottom) cerebella highlight the decreased size of the sagittal plane area of the cerebellar vermis, increased length of the mutant cerebellum, and the abnormal morphology of the lateral portions of the lobes. Left to right is lateral to mid-sagittal. Immunostaining for a marker for GCPs (NeuN, green) and a marker for Purkinje cells (Calbindin1 (CALB1), red) was performed to highlight the morphology of the cerebellum. Scale bar, 500 μm.

(J-R) Developmental time course of control and *Cdc42* cKO cerebella from embryonic age (E) 16.5 through postnatal day (P)15. (J-Q) Mid-sagittal cryostat sections and lateral sagittal section (R) from embryonic and postnatal mice were immunostained with the neuronal marker NeuN and the Purkinje cell marker Calbindin (CALB1). Although there was no difference in size at E16.5, the size of mutant cerebella decreased: 16%, 26%, and 55% at P0, P7 and P15, respectively, compared to control cerebella, and lateral sagittal sections of P15 mice revealed an undulating pattern of the principal layers of the cerebellum in mutant mice. Scale bar, 100 μm.

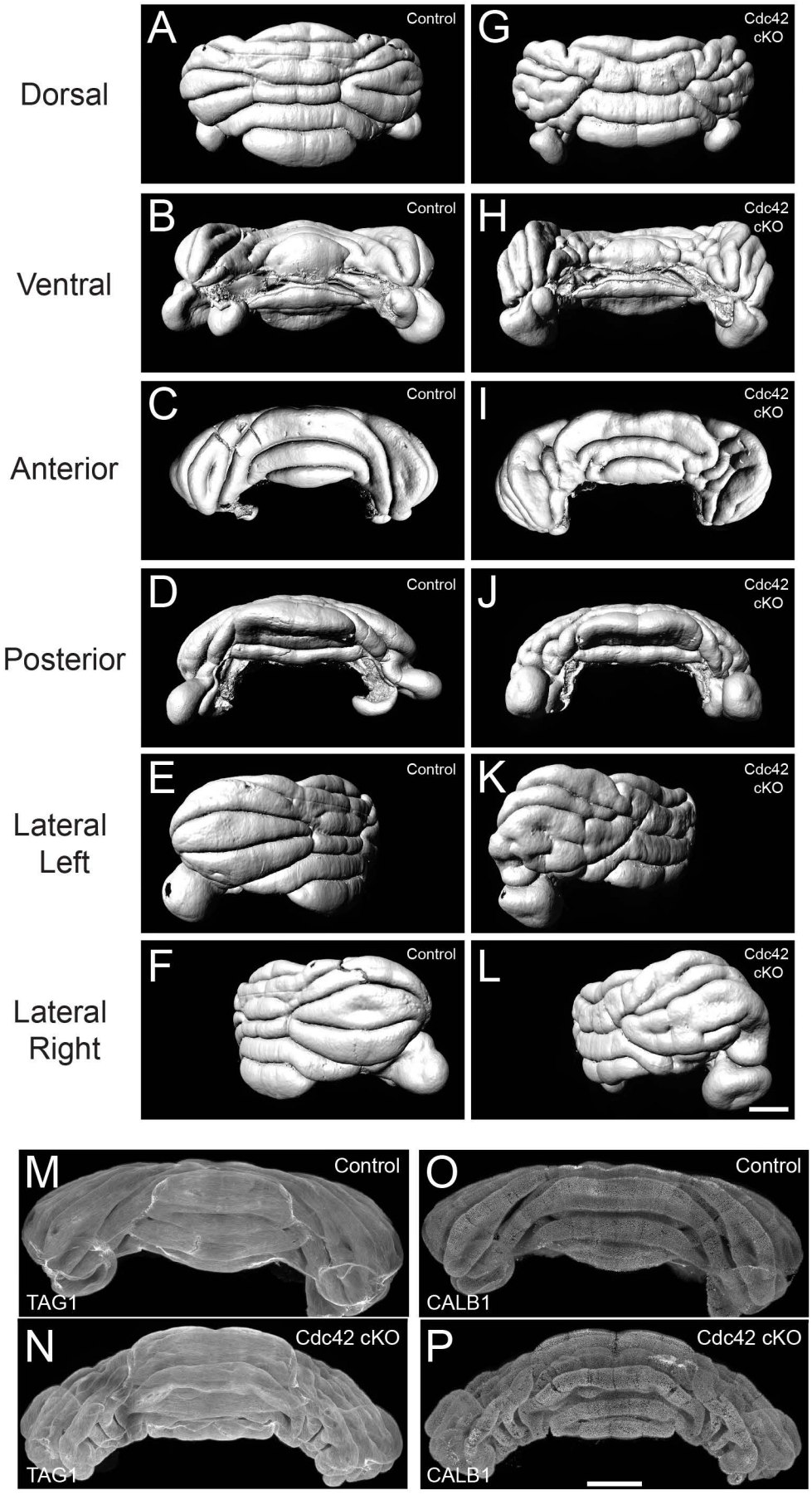
Dorsal
Ventral
Anterior
Posterior
Lateral Left
Lateral Right
A
Control
G
Cdc42 cKO
B
Control
H
Cdc42 cKO
C
Control
I
Cdc42 cKO
D
Control
J
Cdc42 cKO
E
Control
K
Cdc42 cKO
F
Control
L
Cdc42 cKO
M
Control
TAG1
O
Control
CALB1
N
Cdc42 cKO
TAG1
P
Cdc42 cKO
CALB1

Figure S3. iDISCO Clearing, Volumetric Imaging, and Computer Rendering of P7 Cerebella Revealed Defects in Foliation Patterning in the *Cdc42* cKO. Related to Figure 1.

(A-L) Whole cerebella from *Cdc42* cKO (G-L) and control mice (A-F) were cleared using iDISCO methodology, immunostained for TAG1, imaged using light sheet microscopy and computer rendered to reveal the tissue surface and foliation patterning. Scale bar, 1 mm.

(M-P) Whole cerebella from control (M,O) and *Cdc42* cKO (N,P) mice were cleared using iDISCO methodology, immunostained for TAG1 (M,N) or CALB1 (O,P), and imaged using light sheet microscopy. Volume image stacks were projected along the anterior-posterior axis to reveal the tissue surface and foliation patterning. Scale bar, 1 mm.

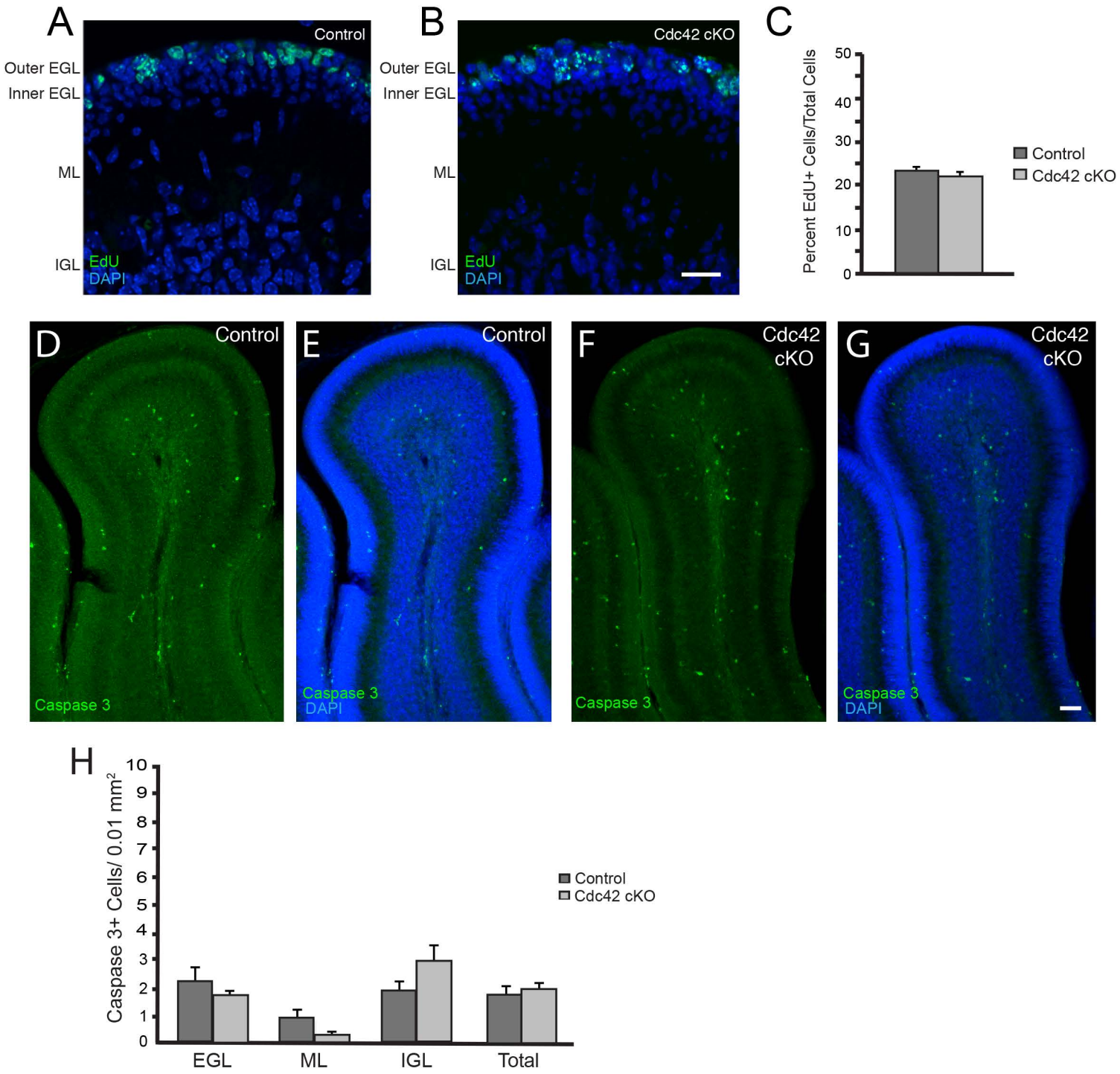
A
Control
Outer EGL
Inner EGL
ML
IGL
EdU
DAPI
B
Cdc42 cKO
Outer EGL
Inner EGL
ML
IGL
EdU
DAPI
C
Percent EdU+ Cells/Total Cells
50
40
30
20
10
0
Control
Cdc42 cKO
D
Control
Caspase 3
E
Control
Caspase 3
DAPI
F
Cdc42 cKO
Caspase 3
G
Cdc42 cKO
Caspase 3
DAPI
H
Caspase 3+ Cells/ 0.01 mm2
10
9
8
7
6
5
4
3
2
1
0
Control
Cdc42 cKO
EGL
ML
IGL
Total

Figure S4. Loss of Cdc42 in GCPs Does Not Affect Postnatal GCP Proliferation or Apoptosis. Related to Figure 1.

(A-C). No difference in the percentage of EdU positive cells in the external granule layer (EGL) of the cerebellar cortex of P7 control or *Cdc42* cKO mice injected with EdU for 1 hour. (A,B) EdU (green) labels cells undergoing DNA replication during proliferation and DAPI (blue) labels all nuclei. (C) Quantitation of the percentage of EdU positive cells in the EGL of control and mutant mice shows no significant difference between the two conditions. Scale bar, 30 μm. Data are represented as mean ± SEM.

(D-H) No difference in the amount of apoptosis in the cerebellar cortex of P7 control or *Cdc42* cKO mice. (D-G) Caspase 3 immunostaining (green) and (E,G) DAPI staining (blue) shown in cerebellar lobules IV/V of control (D,E) and *Cdc42* cKO (F,G). (H) Quantitation of the number of Caspase 3 positive cells in the EGL, ML, IGL, or the sum of cells in all three regions per area in control and mutant mice shows no significant difference between the two conditions. Scale bar, 30 μm. Data are represented as mean ± SEM.

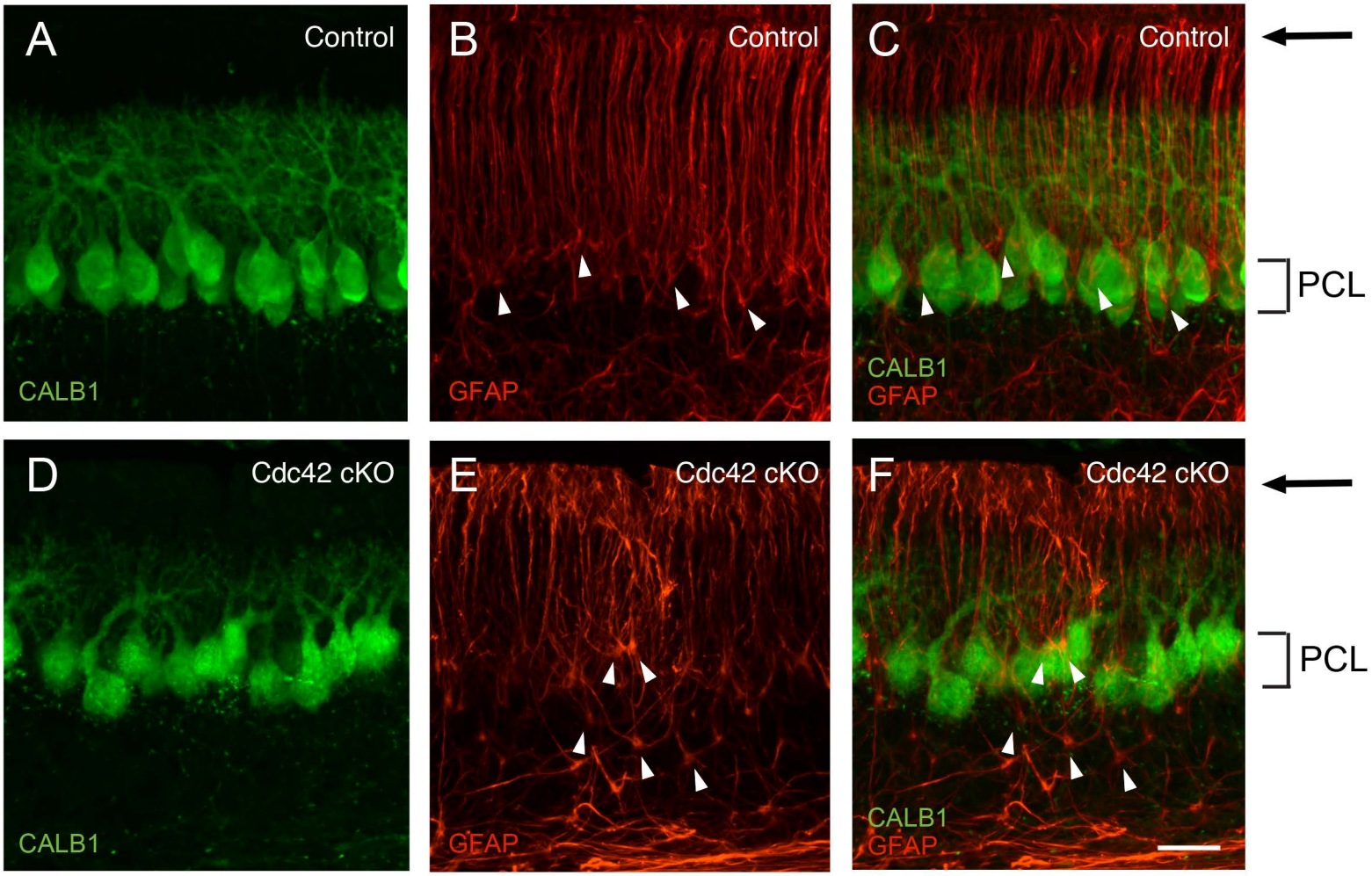
A
Control
CALB1
B
Control
GFAP
C
Control
CALB1
GFAP
PCL
D
Cdc42 cKO
CALB1
E
Cdc42 cKO
GFAP
F
Cdc42 cKO
CALB1
GFAP
PCL

Figure S5. Cell Bodies of Bergmann Glia in Mutant Cerebella are Mis-localized. Related to Figure 5. (A-F) P8 cerebellar sections from control (A-C) and *Cdc42* cKO (D-F) mice were immunostained for GFAP (red) to label glial cells and CALB1 (green) to label PCs. GFAP fibers that span the cerebellar cortex in control mice are disorganized in mutant mice, and BG cell bodies, denoted by arrowheads, are mis-localized in *Cdc42* cKO animals and do not align along the PC layer as in control animals. Arrows point to the ends of the glial fibers, which appeared to be thickened and aberrantly fenestrated in *Cdc42* cKO animals compared to control animals. Scale bar, 30 μm. PCL, Purkinje cell layer.

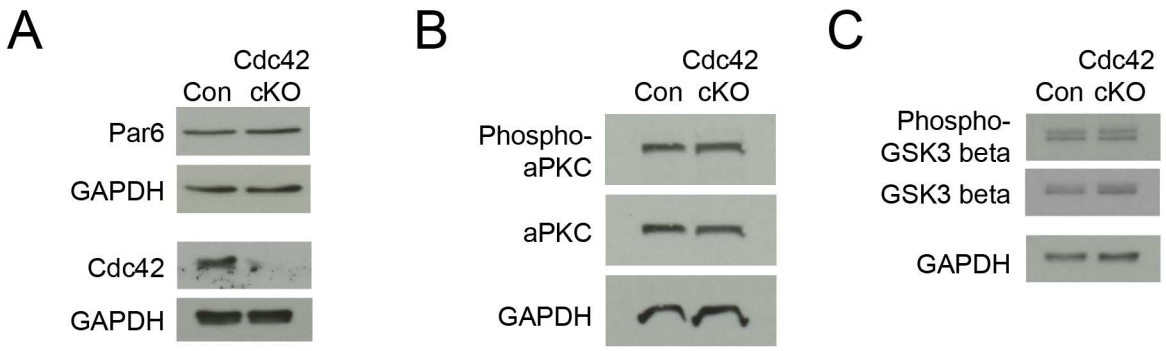
A
Cdc42
Con cKO
Par6
GAPDH
Cdc42
GAPDH
B
Cdc42
Con cKO
Phospho-
aPKC
aPKC
GAPDH
C
Cdc42
Con cKO
Phospho-
GSK3 beta
GSK3 beta
GAPDH

Figure S6. No changes in mPar6 levels, aPKC phosphorylation, or GSK3β phosphorylation were detected on loss of *Cdc42* in GCPs. Related to Table 1.
(A) GCPs isolated from control (Con) and *Cdc42* cKO mice were immunoblotted for Par6 and Cdc42 proteins, and GAPDH as a loading control.
(B) GCPs isolated from control (Con) and *Cdc42* cKO mice were immunoblotted for phospho-aPKC, total aPKC, and GAPDH as a loading control.
(C) GCPs isolated from control (Con) and *Cdc42* cKO mice were immunoblotted for phospho-GSK3β, total GSK3β, and GAPDH as a loading control.

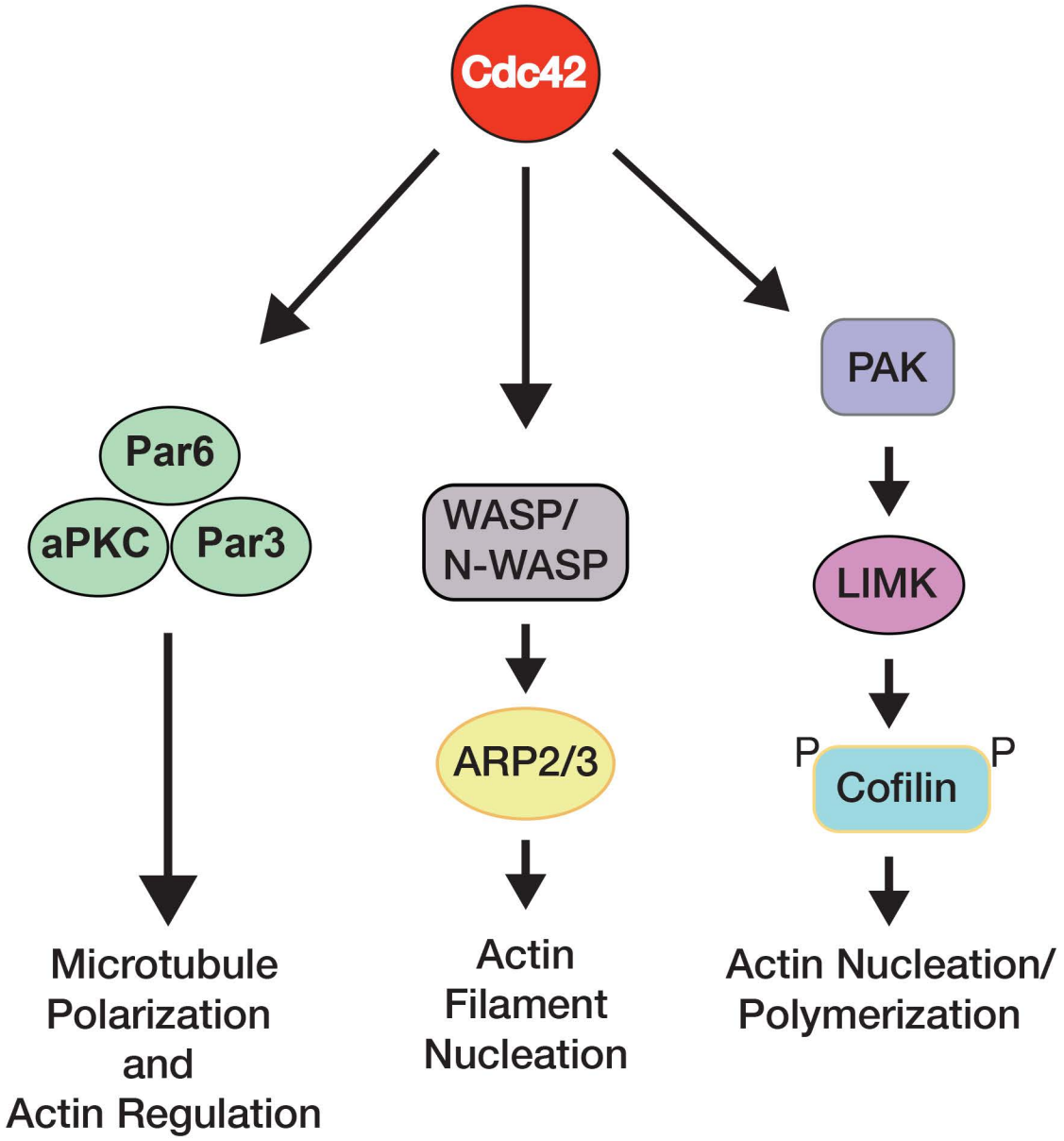
Cdc42
Par6
aPKC
Par3
WASP/
N-WASP
ARP2/3
PAK
LIMK
P
P
Cofilin
Microtubule
Polarization
and
Actin Regulation
Actin
Filament
Nucleation
Actin Nucleation/
Polymerization

Figure S7. Diagram of Main Cdc42 Effector Pathways. Related to Table 1.
The three main effector proteins/pathways of Cdc42 that regulate the cytoskeleton are Par6, Wasp/N-Wasp, and PAK.

Transparent Methods

Animals

C57B1/6J *Cdc42*$^{loxp/loxp}$ mice possessing loxP sites flanking the guanine nucleotide binding sequence coding exon 2 (Chen 2006) were crossed to Swiss Webster *Tg(Atoh1-Cre)*. *Tg(Atoh1-Cre)*$^{+/-}$; *Cdc42*$^{loxp/loxp}$ progeny were then crossed back to C57B1/6J *Cdc42*$^{loxp/loxp}$ mice. *Tg(Atoh1-Cre)*$^{+/-}$; *Cdc42*$^{loxp/loxp}$ mice were compared to *Tg(Atoh1-Cre)*$^{-/-}$; *Cdc42*$^{loxp/loxp}$ control littermates. Genotyping of *Cdc42*$^{loxp/loxp}$ and *Atoh1-Cre* alleles was carried out by PCR and each phenotypic analysis was performed using at least 3 independent litters.

All animal work was performed as required by the United States Animal Welfare Act and the National Institutes of Health's policy to ensure proper care and use of laboratory animals for research, and under established guidelines and supervision by the Institutional Animal Care and Use Committee (IACUC) of The Rockefeller University. Mice were housed in accredited facilities of the Association for Assessment of Laboratory Animal Care (AALAC) in accordance with the National Institutes of Health guidelines.

Constructs and Antibodies

Venus cDNA was PCR generated with the following primers: Venus 5' EcoRI primer GAGAAG GAATTC ACC ATGGTGAGCAAGGGCGAGGAG and Venus 3' NotI primer – stop GAGAAG GCGGCCGC TTACTTGTACAGCTCGTCCATGCCG. The PCR product was inserted into pCIG2 (provided by Dr. Franck Polleux) digested with EcoRI and NotI. Venus fusions of Cdc42 were created by first PCR generating Venus cDNA using the following primers: Venus 5' EcoRI primer GAGAAG GAATTC ACC ATGGTGAGCAAGGGCGAGGAG and Venus 3' BamHI primer GAGAAG GGATCC CTTGTACAGCTCGTCCATGCCGA. The PCR product was inserted into a pMSCXβ plasmid digested with EcoRI and BamHI. Cdc42N17 and Cdc42V12 cDNAs were PCR generated from pCDNA constructs (provided by Dr. Linda Van Aelst) using the following primers: Cdc42 5' BamHI primer GAGAAG GGATCC ACC ATGCAGACAATTAAGTGTGTTGTTGTGG and Cdc42 3' NotI primer GAGAAG GCGGCCGCTTAGAATATACAGCACTTCCTTTTGGGTTGA. The PCR product was then inserted into the BamHI and NotI sites of the pMSCXβ plasmid containing the Venus cDNA without a stop codon and was fused in frame with the 3' end of the Venus cDNA. The Venus fusions of Cdc42 were then digested from the pMSCXβ plasmid and inserted into the EcoRI and NotI sites of the pCIG2 plasmid.

Primary antibodies used for immunofluorescence included rabbit anti-GFP (Invitrogen, 1/2000), goat anti-NeuroD (N19) (Santa Cruz, 1/100), mouse anti-β-tubulin 2.1 (Sigma, 1/2000), rabbit anti-Ki67 (Vector, 1:200), sheep anti-BrdU (Abcam, 1/100), rabbit anti-GFAP (Dako, 1/500), mouse anti-NeuN (Chemicon, 1/200), mouse anti-Calbindin (CALB1) (Swant, 1/1000), rabbit anti-Cre (Novagen, 1/2000), and rabbit anti-active Caspase 3 (Cell Signaling Technology, 1/400). Secondary antibodies used included donkey anti-goat Alexa Fluor® 488 IgG (H+L) (Invitrogen, 1/500), donkey anti-mouse Alexa Fluor® 594 IgG (H+L) (Invitrogen, 1/500), donkey anti-mouse Alexa Fluor® 488 IgG (H+L) (Invitrogen, 1/500), donkey anti-rabbit Alexa Fluor® 594 IgG (H+L) (Invitrogen, 1/500), donkey anti-rabbit Alexa Fluor® 488 IgG (H+L) (Invitrogen, 1/500) and donkey anti-sheep Alexa Fluor® 488 IgG (H+L) (Invitrogen, 1/500).

Antibodies used for Western blotting included rabbit anti-Cdc42 (Santa Cruz, 1/100), goat anti-Pard6a (Santa Cruz, 1/200), rabbit anti-phospho-PKCζ/λ (Thr410/403) (Cell Signaling, 1/1,000), mouse anti-phospho-Y216-GSK3β (BD Transduction, 1/1,000), mouse anti-GSK3β (BD Transduction, 1/5000), mouse anti-GAPDH (Chemicon 1/10,000), etc. Secondary antibodies used included HRP conjugated goat anti-rabbit IgG (H+L) (Bio-Rad, 1/3,000), donkey anti-goat IgG (H+L) (The Jackson Laboratory, 1/10,000), and sheep anti-mouse IgG (H+L) (The Jackson Laboratory, 1/10,000).

Stereoscopic Imaging of Whole Cerebellum for Morphology

P7 cerebella were dissected from the brains of (*Cdc42*$^{loxp/loxp}$) and *Cdc42* cKO (*Tg(Atoh1-Cre)*$^{+/-}$; *Cdc42*$^{loxp/loxp}$) littermate mice and fixed overnight in 4% PFA/4% sucrose/PBS and washed in PBS. The whole cerebellum was then imaged using a Zeiss Axial Imager.A1 microscope.

Size Determination of Sagittal and Coronal Sections

P7 cerebella were dissected from the brains of *Cdc42*$^{loxp/loxp}$ and *Cdc42* cKO (*Tg(Atoh1-Cre)*$^{+/-}$; *Cdc42*$^{loxp/loxp}$) littermate mice in HBSS containing 2.5 mM HEPES (pH 7.4), 46 mM D-glucose, 1 mM $CaCl_2$, 1 mM $MgSO_4$, 4 mM $NaHCO_3$, and Phenol Red. They were then embedded in 3% agarose in HBSS containing 2.5 mM HEPES (pH 7.4), 30 mM D-glucose, 1 mM $CaCl_2$, 1 mM $MgSO_4$, 4 mM $NaHCO_3$, and Phenol Red, and 250 µm coronal sections were made using a Leica VT1000S vibratome set at a speed of 3 and frequency of 6. The acute slices were then fixed with 4% PFA/4% sucrose/PBS for 2 hours at room temperature and immunostained for NeuroD (goat, Santa Cruz, 1/100) and β-tubulin 2.1 (mouse, Sigma, 1/2000) described as below. The sagittal sections were imaged using a Zeiss Axial Imager.A1 microscope and the area and width of sections were measured using the "measurement" tool in Adobe Photoshop software. For the graphs in Figure 1J and Figure 1K, mid-sagittal sections from 5 animals for each condition were measured (n=5).

Serial Sections of Cerebella

To make serial sections of P7 control and conditional Cdc42 knockout cerebella, littermate mice were perfused with 4% PFA/PBS, and the brains were removed, post-fixed in 4% PFA/PBS overnight, and washed in PBS. The brains were then embedded in 3% agarose in PBS and 60 µm sagittal sections were made using a Leica VT1000S vibratome. The sections were immunostained for GFAP (rabbit, Dako, 1/500) to label glial cells and NeuN (mouse, Chemicon, 1/100) to label GCPs. They were imaged using a Zeiss Axioplan 2 microscope fitted with a SPOT (Diagnostics Instruments) Digital Camera system.

EdU Proliferation Assay

P7 control and Cdc42 cKO mice were injected with 50 μg of EdU in PBS per gram of body weight in the back of the head over the cerebellum, sacrificed one hour later, and the cerebella were removed and fixed in 4% PFA/PBS overnight. The cerebella were then washed in PBS, embedded in 3% agarose in PBS, and 50 µm sagittal sections were made using a Leica VT1000S vibratome set at a speed of 3 and frequency of 6. The sections were processed for EdU staining using a Click-iT EdU Imaging Kit (ThermoFisher Scientific) and stained with DAPI to label GCP nuclei. The sections were then imaged using confocal microscopy. The number of EdU positive cells and total GCPs in the EGL were counted and the percentage of EdU positive cells was calculated. For the EdU proliferation graph in Figure S4C, 4299 cells total were counted from 3 animals (n=3) for the control condition and 2993 cells total were counted from 3 animals (n=3) for the *Cdc42* cKO condition.

Caspase 3 Apoptosis Assay

P7 control (*Cdc42*$^{loxp/loxp}$) and *Cdc42* cKO (*Tg(Atoh1-Cre)*$^{+/-}$; *Cdc42*$^{loxp/loxp}$) mice were perfused with 4% PFA/PBS, and the brains were removed and post-fixed in 4% PFA/PBS overnight. The cerebella were then washed in PBS, embedded in 3% agarose in PBS, and 50 µm sagittal sections were made using a Leica VT1000S vibratome set at a speed of 3 and frequency of 6. The sections were immunostained with rabbit anti-active Caspase 3 (Cell Signaling Technology, 1/400) and stained with DAPI to visualize nuclei and distinguish the different layers of the cerebellar cortex. The sections were then imaged by confocal microscopy. The areas of the different layers of the cerebellar cortex were measured in microns using the measurement tool in Adobe Photoshop, the number of Caspase 3 positive cells was counted per area, and the number of Caspase 3 positive cells per area was determined. For the apoptosis graph in Figure S4H, areas for each region of the cerebellar cortex were measured and Caspase 3 positive cells counted for 3 animals (n=3) for the control condition and 3 animals (n=3) for the *Cdc42* cKO condition.

Electroporation of Constructs into Cerebellum and Organotypic Slices

For the DN and CA Cdc42 experiments, brains were dissected from wild type mice in in HBSS containing 2.5 mM HEPES (pH 7.4), 30 mM D-glucose, 1 mM $CaCl_2$, 1 mM $MgSO_4$, 4 mM $NaHCO_3$, and Phenol Red (hereto referred to as HBSS with regular glucose). 2.5 µg/µl of DNA containing Fast Green was injected with a picospritzer (Picospritzer III, Parker Instruments) between the lobes of the cerebellum, and the cerebellum was electroporated dorsal to ventral at 60V using gold paddles (Genepaddles, Genetronics Inc.) and an *electro-square*-porator, *ECM* 830 (BTX Genetronics). The cerebella were then placed on ice for 10 minutes to recover, and subsequently, the cerebellum was dissected from the brain in HBSS containing regular glucose.

For all other experiments involving Venus only, P8 cerebella from *Cdc42*$^{loxp/loxp}$ and *Cdc42* cKO (*Tg(Atoh1-Cre)*$^{+/-}$*; Cdc42*$^{loxp/loxp}$) littermate mice were dissected from brain. The cerebella were dissected out in HBSS containing 2.5 mM HEPES (pH 7.4), 46 mM D-glucose, 1 mM $CaCl_2$, 1 mM $MgSO_4$, 4 mM $NaHCO_3$, and Phenol Red (hereto referred to as HBSS with extra glucose) on ice. The dissection medium was then removed and DNA was diluted to 0.5 µg/µl in HBSS with extra glucose. The cerebella were soaked in the DNA for 15-20 minutes on ice, and were then transferred one at a time into the well of an electroporation chamber (Protech International Inc. CUY520P5 platinum electrode L8xW5xH3 5mm gap) that was placed on ice. The cerebella were electroporated dorsal to ventral for 50 ms at 80 V, for a total of 5 pulses with an interval of 500 ms between pulses, using an *electro-square*-porator, *ECM* 830 (BTX Genetronics). The cerebella were then removed from the chamber and placed on ice to recover for 10 minutes.

Subsequent to electroporation for both DN and CA Cdc42 experiments and the Venus only experiments, the cerebella were embedded in 3% agarose in HBSS containing regular glucose, and 250 µm coronal slices were made using a Leica VT1000S vibratome set at a speed of 3 and frequency of 6. Slices were then placed on MILLICELL CM 0.4 um culture plate inserts in a 6 well plate with 1.5 ml of culture medium (BME, 25 mM D-glucose/1x Glutamine/1x ITS/1x Pen-Strep) below the insert. The organotypic slices were incubated at 35˚C/5% CO_2 60 (Venus only experiments) to 72 (DN and CA Cdc42 experiment) hours before fixing with 4% PFA/4% sucrose/PBS for 2 hours at room temperature. Immunostaining was then performed as described below. The DN and CA Cdc42 experiment slices were imaged with a Carl Zeiss Axioplan2/Bio-Rad Radiance 2000 confocal laser-scanning microscope equipped with a 63x objective, and slices for Venus only experiments were imaged with a Carl Zeiss Axiovert 200M/ Perkin Elmer Ultraview spinning disk confocal microscope equipped with a 25x objective.

Polarity Experiments

P8 control and mutant cerebella were isolated and electroporated with a pCIG2 Venus-expression plasmid to visualize developing and migrating GCPs as described in the "*Electroporation of Constructs into Cerebellum and Organotypic Slices"* section of the Transparent Methods section. 60 hours after electroporation, the slices were fixed and processed for immunostaining with rabbit anti-GFP (Invitrogen, 1/2000) and mouse anti-Calbindin (CALB1, Swant, 1/1000) antibodies, and stained with DAPI, as described in the "*Immunostaining"* section of the Transparent Methods section. Co-immunostaining slices with mouse anti-Calbindin (Swant, 1/1000) to visualize the Purkinje cell layer (PCL) and Dapi to define the EGL and IGL (not shown) aided in defining the EGL, ML, and PCL of the cerebellar cortex (not shown). The slices were then imaged with a Carl Zeiss Axiovert 200M/ Perkin Elmer Ultraview spinning disk confocal microscope equipped with a 25x objective. For quantitation of the polarity experiments in Figure 3E, Venus positive cells were counted and categorized as bipolar or multipolar in the Molecular Layer and Purkinje Cell layer of organotypic cerebellar slices and the percentage of each category was calculated. Bipolar cells were classified as those that had two processes and multipolar cells were those that had more than two processes. A total of 234 (n=234) cells from 5 animals were counted for the control condition and 84 cells (n=84) from 4 animals were counted for the mutant condition.

BrdU Analysis

50 µg of BrdU in PBS per gram of weight was injected underneath the skin in the back of the head over the cerebellum in P5 control (*Cdc42*$^{loxp/loxp}$) and conditional *Cdc42* knockout (*Tg(Atoh1-Cre)*$^{+/-}$*; Cdc42*$^{loxp/loxp}$) mice, and the mice were perfused with 4% PFA/PBS 72 hours later. The brains were removed, post-fixed in 4% PFA/PBS overnight, washed in PBS, soaked in 15% sucrose/PBS for several hours until they sank, and then soaked in 30% sucrose/PBS overnight. The brains were then embedded in Richard-Allan Scientific Neg-50™ Frozen Section Medium (Thermo Scientific) and 16 µm sagittal sections were made using a Leica CM 3050S cryostat. Mid-sagittal sections were first immunostained for Ki67 (rabbit, Vector, 1/200) or GFAP (rabbit, Dako, 1/500) as described in the "Immunostaining" Transparent Methods section. Subsequently, the sections were processed for BrdU immunostaining. The sections were washed 3x in 1x PBS, 5 minutes each time, and then were incubated in 2N HCl for 30 minutes at 37˚C. The sections were then washed again 3x in 1x PBS, 5 minutes each time, and incubated in 0.1 M Na Borate, pH 8.5 for 10 minutes at room temperature. The sections were blocked with 10% NDS/0.5% Triton X-100/PBS for 1 hour at room temperature and then incubated with sheep anti-BrdU antibody 1/100 in incubation medium (3% NDS/0,01% Triton X-100/PBS) overnight at 4˚C. The sections were then washed 3x with PBS, 5

minutes each time and incubated with donkey anti-sheep Alexa Fluor® 488 IgG (H+L) (Invitrogen, 1/500) secondary antibody for 1 hour at room temperature. The sections were then washed 3x with PBS and mounted with Molecular Probes ProLong® Gold anti-fade mounting media (Invitrogen). The sections were imaged with a Carl Zeiss Axiovert 200M/ Perkin Elmer Ultraview spinning disk confocal microscope, and the number of BrdU+ cells in the EGL, ML, and IGL of the cerebellar cortex of control and *Cdc42* cKO animals were counted using the "count" tool in Photoshop and the percentages in each area determined. A total of 2293 (n=2293) cells from 4 animals were counted for the control condition and 1595 cells (n=1595) from 4 animals were counted for the mutant condition. The thickness of the different regions of the cerebellar cortex in control and Cdc42 cKO animals were also measured using the "ruler" tool in Photoshop and quantitated. The thickness of the EGL, ML and IGL were measured from sections for 4 animals for each condition (n=4).

Glial Fiber and Purkinje Cell Analysis

For glial fiber analysis, mid-sagittal sections from the BrdU experiments were first immunostained for GFAP (rabbit, Dako, 1/500) as described in the "Immunostaining" Transparent Methods section and subsequently were processed for BrdU immunostaining as described in the "*BrdU Analysis*" Transparent Methods section above. Matching serial sections from P7 control and conditional *Cdc42* knockout littermate mice were compared. Briefly, the mice were perfused with 4% PFA/PBS, and the brains were removed, post-fixed in 4% PFA/PBS overnight, and washed in PBS. The brains were then embedded in 3% agarose in PBS and 60 μm sagittal sections were made using a Leica VT1000S vibratome. The sections were immunostained for GFAP (rabbit, Dako, 1/500) to label glial cells and NeuN (mouse, Chemicon, 1/100) to label GCPs.

For PC analysis, P7 control and conditional *Cdc42* knockout littermate mice were perfused with 4% PFA/PBS, and the brains were removed, post-fixed in 4% PFA/PBS overnight, and washed in PBS. The brains were then embedded in 3% agarose in PBS and 60 μm serial sagittal sections were made using a Leica VT1000S vibratome. The sections were immunostained for Calbindin (CALB1, mouse, Swant, 1/1000) to label Purkinje cells.

Images were taken with a Carl Zeiss Axiovert 200M/Perkin Elmer Ultraview spinning disk confocal microscope equipped with a 25x objective.

Immunostaining

For immunostaining of organotypic slices or floating vibratome sections, the slices or sections were permeabilized and blocked overnight in 1x PBS/0.3% Triton X-100/10% Normal Donkey Serum (NDS). The sections were then incubated overnight with primary antibodies diluted in 1x PBS/0.3% Triton X-100/10% NDS. Subsequently, the sections were washed 3 times for 20 minutes each in 1x PBS/0.3% Triton X-100/10% NDS and incubated overnight with Alexa Fluor® conjugated secondary antibodies diluted in 1x PBS/0.3% Triton X-100/10% NDS. The sections were then washed 4 times 30 minutes each time, any remaining agarose was carefully removed, and the sections were mounted with Molecular Probes ProLong® Gold anti-fade mounting media (Invitrogen).

For immunostaining cryostat sections on slides, the sections/slides were rinsed 3 times in 1x PBS, blocked 1 hour in 3% NDS/0.1% Triton X-100/1x PBS, and incubated overnight with primary antibodies diluted in 3% NDS/0.01% Triton X-100/1x PBS. The following day, the sections were washed 3-4 times, 10-15 minutes each wash, in 0.1% Triton X-100/1x PBS, incubated 1 hour in Alexa Fluor® conjugated secondary antibodies diluted in 3% NDS/0.01% Triton X-100/1x PBS, washed 3-4 times, 10-15 minutes each wash, in 0.1% Triton X-100/1x PBS, and mounted with Molecular Probes ProLong® Gold anti-fade mounting media (Invitrogen).

Whole mount P7 cerebellum analysis with a modified iDISCO procedure

P7 cerebella were dissected and fixed in 4%PFA/1xPBS at 4°C overnight, then washed with 1xPBS/0.02%NaN3 for three times at room temperature. The samples were permeabilized with 0.3M glycine/0.1% Triton X-100/1xPBS at room temperature overnight, then delipidated with methanol gradients (methanol diluted in 0.01xPBS): 20%, 40%, 60%, 80%, 100%, 100%, 80%, 60%, 40%, 20%, with 30

minutes for each step. The samples were then washed in 5%DMSO/0.3M glycine/2ug/ml heparin/0.1% Triton X-100/0.05% Tween-20/1xPBS for 1 hour, and in 2ug/ml heparin/0.1% Triton X-100/0.05% Tween-20/1xPBS for 1hour three times. The samples were incubated with primary antibodies, goat anti-TAG1 (R&D systems, 1/100) and rabbit anti-CALB1 (Swant CB38, 1/100), diluted in 2ug/ml heparin/0.1% Triton X-100/0.05% Tween-20/1xPBS, at 37°C for 2 days. Samples were washed for 1 day, then incubated with secondary antibodies, donkey anti-mouse Alexa Fluor® 647 IgG (H+L) (Invitrogen, 1/100) and donkey anti-rabbit Alexa Fluor® 568 IgG (H+L) (Invitrogen, 1/100), at 37°C for 2 days. After washing for 2 days, samples were embedded in 1% agarose/1xPBS, then dehydrated with methanol gradient (from 20% to 80%), then 100% methanol, DCM, and DBE for clearing. Cleared samples were imaged with LaVision light-sheet fluorescent microscope with 4x objective lens. The volume image stacks were imported into Imaris x64 software (version 8.0.1, Bitplane) to generate surface contour based on TAG1 staining to visualize foliation organization in 3D, and coronal max-intensity-projection for both TAG1 and CALB1 staining to correlate the foliation defects.

Electron Microscopy

P7 control and conditional *Cdc42* knockout littermate mice were perfused with saline followed by 2% paraformaldehyde and 2.5% glutaraldehyde in 0.1M sodium cacodylate buffer (pH 7.4) at room temperature. The brains were removed and immersed in the fixative overnight. The following day, the posterior portion of the brain with the cerebellum was isolated and 500 μm sections were made using a Leica VT100S vibratome. The sections were then stored in 2.5% glutaraldehyde in 0.1M sodium cacodylate buffer (pH 7.4) at 4˚C.

Cerebellar sections were washed in 0.1M sodium cacodylate buffer (pH 7.4), and post-fixed with 2.5% glutaraldehyde/0.25% tannic acid in 0.1M sodium cacodylate buffer for 15 minutes. They were then fixed with 2.5% glutaraldehyde in 0.1M sodium cacodylate buffer for 15 minutes and with 1% osmium tetra-oxide in sodium cacodylate buffer for 30 min on ice. The sections were subsequently washed three times in 0.1M sodium cacodylate buffer (pH 7.4) for 5 min and rinsed three times with water. They were then stained with 1% uranyl acetate for 30 min at room temperature followed by 12 hours on ice. The sections were dehydrated in an increasing concentration of ethanol; 50%, 70%, 90%, 100%, and 100% using Pelco Biowave Pro microwave automatic protocol (TedPella, Inc.). They were then infiltrated with Epon812 resin, using an increasing concentration of resin in acetone; 50%, 100%, and 100% using Pelco Biowave Pro microwave automatic protocol (TedPella, Inc.). The sections were infiltrated with Epon812 for 24 hours on a rotating rack, and the resin was replaced three times before polymerization for 48 hours at 60°C. Areas of interest in cerebellar lobe 4/5 were then selected under the light microscope and trimmed for microtome sectioning. 70 nm sections were cut and collected on electron microscope grids, and samples were counter-stained using 1% uranyl acetate and Sato's lead stain (Proc. XIth Int. Cong. on Electron Microscopy. Kyoto. 1986, pp. 2181-2182). The sections were then imaged with 2500-5000x magnification using 120kV operated Jeol 1400 plus TEM or Tecnai G2 TEM. Montage images were collected using SerialEM software and aligned using IMOD software.

Western Blotting

GCPs were isolated from P7 cerebella from control and conditional *Cdc42* knockout littermates as previously described using Percoll gradient sedimentation (Hatten 1989), washed with ice-cold PBS, spun for 5 minutes at 2500 rpm and lysed with ice-cold Triton X-100 lysis buffer containing protease and phosphatase inhibitors (50 mM Tris HCl, pH 7.5; 100 mM NaCl; 50 mM NaF; 5 mM EDTA; 1% Triton X-100; 40 mM β-glycerophosphate; 200 μM Na Orthovanadate; 100 μM PMSF; 1/100 Sigma Protease Inhibitor Cocktail (PIC) P8340; EMD Millipore Phosphatase Inhibitor Cocktail Set II 1/100; EMD Millipore Phosphatase Inhibitor Cocktail Set IV 1/200). The cells in lysis buffer were gently triturated several times, incubated 20 minutes on ice, gently triturated several times again, and spun for 20 minutes at 14,000 rpm at 4˚C. The supernatant was removed, a small aliquot set aside to determine the protein concentration, and the rest of the sample was snap frozen in liquid nitrogen and stored at -80˚C. Protein concentrations were determined using the Pierce BCA Protein Assay Kit (Thermo Scientific). Normalized lysates containing Laemmli sample buffer were boiled for 5 minutes and separated on SDS-polyacrylamide electrophoresis gels, transferred onto Immobilin-P PVDF membrane (Millipore), and immunoblotted using standard methods.

Antibodies used for Western blotting included rabbit anti-Cdc42 (Santa Cruz, 1/100), goat anti-Pard6a (Santa Cruz, 1/200), rabbit anti-phospho-PKCζ/λ (Thr410/403) (Cell Signaling, 1/1,000), rabbit anti-PKCζ (Abcam, 1/500), mouse anti-phospho-Y216-GSK3β (BD Transduction, 1/1,000), mouse anti-GSK3β (BD Transduction, 1/5000), mouse anti-GAPDH (Chemicon 1/10,000), and rabbit anti-Cre (Novagen, 1/10,000). Secondary antibodies used included HRP conjugated goat anti-rabbit IgG (H+L) (Bio-Rad, 1/3,000), donkey anti-goat IgG (H+L) (The Jackson Laboratory, 1/10,000), and sheep anti-mouse IgG (H+L) (The Jackson Laboratory, 1/10,000).

RNA-Seq

GCPs were isolated from P7 cerebella for 5 control and 5 conditional *Cdc42* knockout littermates as previously described using Percoll gradient sedimentation (Hatten 1989), and RNA was isolated using a Qiagen RNeasy miniprep kit. RNA samples with RNA Integrity Numbers (RINs) above 9 were submitted to the Rockefeller Genomics Resource Center, which then prepared the cDNA libraries and carried out the sequencing.

100 ng of total RNA was used to generate RNA-Seq libraries using Illumina TruSeq RNA Sample Prep kit v2 (Cat# RS-122-2001). Libraries prepared with unique barcodes were pooled at equal molar ratios. The pool was denatured and sequenced on Illumina HiSeq 2000 or HiSeq 2500 sequencers to generate 100 bp single reads, following manufacturers' protocols.

RNA-seq reads were aligned to the reference mouse genome (mm10) with the aligner STAR. Genes annotated in gencode vM2 were quantified with featureCounts and differential gene expression was performed with the R package DESeq2, which is based on a negative binomial distribution.

Global Phosphoproteomics and Pathway Analysis

GCPs were isolated from P7 cerebella from control and conditional *Cdc42* knockout littermates as previously described using Percoll gradient sedimentation (Hatten 1989), washed with ice-cold PBS, spun for 5 minutes at 2500 rpm and lysed with ice-cold Triton X-100 lysis buffer containing protease and phosphatase inhibitors (50 mM Tris HCl, pH 7.5; 100 mM NaCl; 50 mM NaF; 5 mM EDTA; 1% Triton X-100; 40 mM β-glycerophosphate; 200 µM Na Orthovanadate; 100 µM PMSF; 1/100 Sigma Protease Inhibitor Cocktail (PIC) P8340; EMD Millipore Phosphatase Inhibitor Cocktail Set II 1/100; EMD Millipore Phosphatase Inhibitor Cocktail Set IV 1/200). The cells in lysis buffer were gently triturated several times, incubated 20 minutes on ice, gently triturated several times again, and spun for 20 minutes at 14,000 rpm at 4˚C. The supernatant was removed, a small aliquot set aside to determine the protein concentration, and the rest of the sample was snap frozen in liquid nitrogen and stored at -80˚C. Protein concentrations were determined using the Pierce BCA Protein Assay Kit from Thermo Scientific. Four replicates for each condition from four different litters were submitted for phospho-proteomic analysis (n=4).

LC-MS/MS

In brief, 200 µg sample per replicate (n=4) were digested and desalted. 2% of each sample was subjected to protein profiling while the remainder was subjected to titanium dioxide based phosphopeptide enrichment followed by quantitation. Both experiments were analyzed by high resolution/high accuracy LC-MS/MS (Fusion Lumos, Thermo Fisher). Only phosphopeptides and proteins measured in 3-of-4 biological replicates for at least one condition was considered for the quantitative analysis. Detailed methods are listed below.

LC-MS/MS Sample Preparation

Samples (each 200 µg per) were ice-cold acetone precipitated overnight. Precipitates were dissolved in 8 M Urea/0.1 M ammonium bicarbonate/20 mM DTT. After 1h incubation at room temperature, reduced cysteines were alkylated (iodoacetamide, Sigma) in the dark for 1h. Volumes were diluted 2-fold and proteins were digested overnight with 6 µg Lysyl Endopeptidase (Wako). Prior to trypsinization (Promega), the samples were further diluted 2-fold (0.1 M ammonium bicarbonate). After 8h, digestion was halted by addition of neat TFA (Sigma). Peptides were desalted and concentrated using C_{18} based solid phase extraction (Oasis WAT094225, Waters) and eluted in 700 µL 80% acetonitrile/6% TFA. 2% of each sample was saved for a quantitative protein profiling experiment. To the remainder, lactic acid was added

to a final concentration of 250 mM (Sugiyama et al., 2007), followed by the addition of 2 mg titanium dioxide beads (Titansphere, GLSciences Inertsil) preconditioned in 80% Acetonitrile/6% TFA. Peptides were incubated under shaking for 2 h at room temperature. Beads were washed 3 times and hereafter transferred to a P200 tip restricted with Empore C_8 membranes (3M). Enriched peptides were eluted from beads in 5% ammonia. The P200 tip and Empore C8 membranes were hereafter washed twice with 80% acetonitrile/1% TFA and the wash volumes were combined with the eluent. Phosphopeptide enriched samples were dried in SpeedVac and dissolved in 10 µL 1% acetonitrile/0.1% TFA prior to LC-MS/MS analysis.

LC-MS/MS Experiment

Phosphopeptide enriched samples were analyzed in technical duplicate. Peptides were separated using a direct-loading setup with a 12 cm packed-in-emitter C_{18} column (inner diameter of 75 µm, Nikkyo Technologies, Japan). Peptides were eluted using a gradient increasing from 2% B/98% A to 40% B/60% A (A: 0.1% formic acid, B: 80% acetonitrile/0.1% formic acid) in 140 minutes. Gradient was delivered at 300 nL/min (Easy 1200, Thermofisher). The mass spectrometer (Fusion Lumos, Thermo Fisher) was operated in High/High mode with MS and MS/MS mass resolution being 60,000 and 30,000, respectively. For MS/MS, Automatic Gain Control was set to 1e5 with a maximum injection time of 40 ms. For quantitative protein profiling, peptides were separated using the same gradient but extended to a total of 180 minutes and the mass spectrometer was operated in High/Low mode. For protein quantitation, peptides were separated using a 50 cm EasySprayer (ES80, Themo Fisher).

.

LC-MS/MS Analysis

Data were analyzed using MaxQuant v. 1.6.0.13, Perseus and ProteomeDiscoverer v.1.4.1.14 / MASCOT v. 2.2 / PhosphoRS v.3.0 combined with Percolator.

.

Uniprot's Mouse Complete Proteome (March 2016) concatenated with common contaminants was used for searching. Phosphorylation of Serine, Threonine and Tyrosine, oxidized methionine and protein N-terminal acetylation were allowed as variable modifications (max. of 5 modifications per peptide). Up to 3 missed cleavages were allowed. MS data were mass calibrated followed by a main search using a mass tolerance of 4.5 ppm. False Discovery Rates of 1% were used for both peptide and proteins. Only peptides with a length of 7 or more residues were considered. Approximately 21,000 unique peptides were matched of which 17,671 were phosphorylated. For the quantitative protein profiling of the two conditions ~6,000 proteins were matched. Match between runs was used for all analyses. Technical replicates were merged. Phosphorylation sites changing 2-fold or more are listed in File S2. All raw LC-MS/MS data and peptide identifications have been uploaded to the PRIDE data repository: Project Name: Cdc42 phosphorylation study, Project accession: PXD008148, Username: reviewer79582@ebi.ac.uk, Password: WILJxtepAll .RAW files and matched peptides were deposited at PRIDE.

Protein profiling was quantitated using 'Label Free Quantitation' (LFQ) (Cox et al., 2014) while peptide 'Intensity' was used for the phosphopeptide quantitation. Missing values were manually accessed when signals were fully absent in all 4 replicates. Correlation of peptide intensities in-between samples were between R^2 of 0.71 and R^2 of 0.83).

Analysis Metrics

Samples were on average 91% enriched for phosphopeptides (signal based) and enrichment percentages were consistent in-between samples (standard deviation of 2.3%). For both quantitative analyses, it was required that a peptide/protein must be measured in a minimum 3 of 4 biological replicates in at least one condition. 12,099 phosphopeptides originating from 3,652 proteins could be quantitated and 4,458 proteins were quantitated. Approximately 58 percent of the measured phosphorylated proteins could also be quantitated in the protein profiling experiment.

Pathway Analyses

The **D**atabase for **A**nnotation, **V**isualization and **I**ntegrated **D**iscovery (**DAVID**) program was used for pathway analysis. Any protein with phosphorylation(s) that was either decreased 2-fold (n=883) or increased 2-fold (n=52) was used as input. Additionally, any protein that had phosphorylations that were

identified in at least 3 controls and no knockout samples (n=321) or at least 3 knockout samples and no controls (n=118) was also used.

Statistical Analyses

For the graphs in Figure 1J,K, Figure 3E, and Figure 4E,F, data were presented as mean ± SD or s.e.m. (as indicated in the figure legends) from at least three independent experiments. Direct comparisons were made using Student's t-test. Statistical significance was defined as $P < 0.05$, 0.01 or 0.001 (indicated as *, ** or ***, respectively). P values ≥ 0.05 were considered not significant. For size determination of control and mutant cerebella represented in Figure 1J,K graphs, mid-sagittal sections from 5 animals for each condition were measured for area and width (n=5). For the polarity analysis in the graph of Figure 3E, a total of 234 (n=234) cells from 5 animals were counted for the control condition and 84 cells (n=84) from 4 animals were counted for the mutant condition. For the graph in Figure 4E, a total of 2293 (n=2293) cells from 4 animals were counted for the control condition and 1595 cells (n=1595) from 4 animals were counted for the mutant condition. For the graph in Figure 4F, the thickness of the EGL, ML and IGL were measured from sections for 4 animals for each condition (n=4). For the EdU proliferation graph in Figure S4C, 4299 cells total were counted from 3 animals (n=3) for the control condition and 2993 cells total were counted from 3 animals (n=3) for the *Cdc42* cKO condition. For the Apoptosis graph in Figure S4H, areas for each region of the cerebellar cortex were measured and Caspase 3 positive cells counted for 3 animals (n=3) for the control condition and 3 animals (n=3) for the *Cdc42* cKO condition.